Testing the technicolor interpretation of the CDF dijet excess at the 8-TeV LHC

Estia Eichten, Kenneth Lane, Adam Martin, and Eric Pilon

Phys. Rev. D **86**, 074015 — Published 9 October 2012

DOI: 10.1103/PhysRevD.86.074015

FERMILAB-Pub-12-253-T
LAPTh-025/12

Testing the Technicolor Interpretation of the CDF Dijet Excess at the 8-TeV LHC

Estia Eichten[1*], Kenneth Lane[2†], Adam Martin[1‡] and Eric Pilon[3§]
[1]Theoretical Physics Group, Fermi National Accelerator Laboratory
P.O. Box 500, Batavia, Illinois 60510
[2]Department of Physics, Boston University
590 Commonwealth Avenue, Boston, Massachusetts 02215
[3]Laboratoire d'Annecy-le-Vieux de Physique Théorique
UMR5108 , Université de Savoie, CNRS
B.P. 110, F-74941, Annecy-le-Vieux Cedex, France

August 24, 2012

Abstract

Under the assumption that the dijet excess seen by the CDF Collaboration near 150 GeV in Wjj production is due to the lightest technipion of the low-scale technicolor process $\rho_T \to W\pi_T$, we study its observability in LHC detectors for $\sqrt{s} = 8\,\text{TeV}$ and $\int \mathcal{L}dt = 20\,\text{fb}^{-1}$. We describe interesting new kinematic tests that can provide independent confirmation of this LSTC hypothesis. We show that cuts similar to those employed by CDF, and recently by ATLAS, cannot confirm the dijet signal. We propose cuts tailored to the LSTC hypothesis and its backgrounds at the LHC that may reveal $\rho_T \to \ell\nu jj$. Observation of the isospin-related channel $\rho_T^\pm \to Z\pi_T^\pm \to \ell^+\ell^- jj$ and of $\rho_T^\pm \to WZ$ in the $\ell^+\ell^-\ell^\pm\nu_\ell$ and $\ell^+\ell^- jj$ modes will be important confirmations of the LSTC interpretation of the CDF signal. The $Z\pi_T$ channel is experimentally cleaner than $W\pi_T$ and its rate is known from $W\pi_T$ by phase space. It can be discovered or excluded with the collider data expected by the end of 2012. The $WZ \to 3\ell\nu$ channel is cleanest of all and its rate is determined from $W\pi_T$ and the LSTC parameter $\sin\chi$. This channel and $WZ \to \ell^+\ell^- jj$ are discussed as a function of $\sin\chi$.

*eichten@fnal.gov
†lane@physics.bu.edu
‡aomartin@fnal.gov
§pilon@lapp.in2p3.fr

1. Introduction

The CDF Collaboration has reported evidence for a resonance near 150 GeV in the dijet-mass spectrum, M_{jj}, of Wjj production. This was based on an integrated luminosity of $4.3\,\mathrm{fb}^{-1}$ [1] and updated with a total data sample of $7.3\,\mathrm{fb}^{-1}$ [2]. In Ref. [2], the resonant dijet excess has a significance of $4.1\,\sigma$. The DØ Collaboration, on the other hand, published a search for this resonance based on $4.3\,\mathrm{fb}^{-1}$ that found no significant excess. Based on a W+Higgs boson production model, DØ determined a cross section for a potential signal of $0.82^{+0.83}_{-0.82}\,\mathrm{pb}$ and a 95% confidence level upper limit of 1.9 pb [3]. Analyzing its data with the same production model, CDF reported a signal rate of $3.0\pm0.7\,\mathrm{pb}$ and a discrepancy between the two experiments of $2.5\,\sigma$ [4]. This discrepancy remains. The purpose of this paper is to help guide the LHC experiments in searches to test for the CDF dijet excess in the Wjj and two closely related channels. We do this in the context of low-scale technicolor (LSTC), interpreting CDF's dijet excess as the lightest technipion $\pi_T^{\pm,0}$ of this scenario, produced in association with $W^\pm$ in the decay $\rho_T^{\pm,0}, a_T^{\pm,0} \to W\pi_T$ and decaying to a pair of quark jets [5]. The related channels supporting this interpretation are $\rho_T^\pm, a_T^\pm \to Z\pi_T^\pm$ and $W^\pm Z$.[1] They require *no* additional LSTC model assumptions beyond those made in Ref. [5] to determine LHC production rates. We assume $\sqrt{s} = 8\,\mathrm{TeV}$ and consider $\int \mathcal{L}dt = 20\,\mathrm{fb}^{-1}$, the amount of data expected to be in hand by the end of 2012.[2]

Low-scale technicolor (LSTC) is a phenomenology based on walking technicolor [8, 9, 10, 11]. The gauge coupling α_{TC} must run very slowly for 100s of TeV above the TC scale, $\Lambda_{TC} \sim$ several 100 GeV, so that extended technicolor (ETC) can generate sizable quark and lepton masses while suppressing flavor-changing neutral current interactions [12]. This may be achieved, e.g., with technifermions belonging to higher-dimensional representations of the TC gauge group. Then, the constraints of Ref. [12] on the number of ETC-fermion representations imply that there will be technifermions in the fundamental TC representation as well. They are expected to condense at an appreciably lower energy scale than those belonging to the higher-dimensional representations and, thus, their technipions' decay constant $F_1^2 \ll F_\pi^2 = (246\,\mathrm{GeV})^2$ [13]. Spin-one bound states of these technifermions will have an orthoquarkonium-like spectrum with masses well below a TeV — greater than the previous Tevatron limit $M_{\rho_T} \gtrsim 250\,\mathrm{GeV}$ [14, 15] and probably less than 600–700 GeV, a scale at which we believe the notion of "low-scale" TC ceases to make sense. The most accessible states are the lightest technivectors, $V_T = \rho_T(I^G J^{PC} = 1^+1^{--})$, $\omega_T(0^-1^{--})$ and $a_T(1^-1^{++})$. Through their mixing with the electroweak bosons, they are readily produced as s-channel resonances via the Drell-Yan process in colliders. Spin-zero technipions $\pi_T(1^-0^{-+})$ are accessed in V_T

[1] LHC studies of the Wjj and WZ channels carried out so far are discussed in Secs. 3 and 5, respectively.

[2] Preliminary versions of this paper were circulated in Ref. [6] and Ref. [7] assuming $\sqrt{s} = 7\,\mathrm{TeV}$ and $\int \mathcal{L}dt = 1$–$20\,\mathrm{fb}^{-1}$. The simulations in the current paper may be applied to different luminosities by scaling the event rates. We have not included the nontrivial effects of pileup at the higher luminosities of 8-TeV running. They also make difficult a detailed comparison of our results with the earlier 7-TeV ones. Our signal cross sections are uniformly 20% greater at 8 TeV than at 7 TeV, but the increases in various physics backgrounds are not so simply summarized.

decays. A central assumption of LSTC is that these lightest technihadrons may be treated in isolation, without significant mixing or other interference from higher-mass states. Also, we expect that (1) the lightest technifermions are $SU(3)$-color singlets, (2) isospin violation is small for V_T and π_T, (3) $M_{\omega_T} \cong M_{\rho_T}$, and (4) M_{a_T} is not far above M_{ρ_T}. This last assumption is made to keep the low-scale TC contribution to the S-parameter small. An extensive discussion of LSTC, including these points and precision electroweak constraints, is given in Ref. [16].

Walking technicolor has another important consequence: it enhances M_{π_T} relative to M_{ρ_T} so that the all-π_T decay channels of the V_T are likely to be closed [13]. Principal V_T-decay modes are $W\pi_T$, $Z\pi_T$, $\gamma\pi_T$, a pair of EW bosons (which can include one photon), and fermion-antifermion pairs [17, 18, 16]. If allowed by isospin, parity and angular momentum, V_T decays to one or more weak bosons involve longitudinally-polarized W_L/Z_L, the technipions absorbed via the Higgs mechanism. The rates for these nominally strong decays are suppressed by powers of $\sin^2\chi = (F_1/F_\pi)^2 \ll 1$. This important LSTC parameter is a mixing factor that measures the amount that the lowest-scale technipion is the mass eigenstate π_T ($\cos\chi$) and the amount that it is W_L/Z_L ($\sin\chi$). Thus, each replacement of a mass-eigenstate π_T by W_L/Z_L in a V_T decay amplitude costs a factor of $\tan\chi$. Decays to transversely-polarized $\gamma, W_\perp, Z_\perp$ are suppressed by g, g'. Thus, the V_T are *very* narrow, $\Gamma(\rho_T) \lesssim 1\,\text{GeV}$ and $\Gamma(\omega_T, a_T) \lesssim 0.1\,\text{GeV}$ for the masses considered here. These decays have striking signatures, visible above backgrounds within a limited mass range at the Tevatron and probably up to 600–700 GeV at the LHC [19, 20].

In Ref. [5] we proposed that CDF's dijet excess is due to resonant production of $W\pi_T$ with $M_{\pi_T} = 160\,\text{GeV}$. We took $M_{\rho_T} = 290\,\text{GeV}$ and $M_{a_T} = 1.1M_{\rho_T} = 320\,\text{GeV}$.[3] Then, about 75% of the $W\pi_T$ rate at the Tevatron is due to $\rho_T \to W\pi_T$ and, of this, most of the W's are longitudinally polarized.[4] The remainder is dominated by a_T production. Its decay, and a small fraction of the ρ_T's, involve $W_\perp$ production, which is generated by dimension-five operators [16]. These operators are suppressed by mass parameters $M_{V,A}$ that we take equal to M_{ρ_T}. The other LSTC parameters relevant to $W\pi_T$ production are $g_{\rho_T\pi_T\pi_T}$ and $\sin\chi$. The $\rho_T \to \pi_T\pi_T$ coupling $g_{\rho_T\pi_T\pi_T}$ is the same for all ρ_T decays considered here and it is naively scaled from QCD; its PYTHIA default value is $\alpha_{\rho_T} = g^2_{\rho_T\pi_T\pi_T}/4\pi = 2.16(3/N_{TC})$ with $N_{TC} = 4$. We use $\sin\chi = 1/3$. Using the LSTC model implemented in PYTHIA [17, 18, 21], we found $\sigma(\bar{p}p \to \rho_T \to W\pi_T \to Wjj) = 2.2\,\text{pb}$ (480 fb for $W \to e\nu$, $\mu\nu$).[5] Adopting CDF's cuts, we closely matched its M_{jj} distribution for signal and background. Motivated by the peculiar kinematics of ρ_T production at the Tevatron and $\rho_T \to W\pi_T$ decay, we also suggested

[3] The Pythia default decays for technipions are based on the assumption that they are Higgs-like, i.e., involve couplings proportional to fermion mass. They are thus dominated by $\pi_T^+ \to c\bar{b}$, $u\bar{b}$ and $\pi_T^0 \to b\bar{b}$. These modes involve energy loss to neutrinos that we have not included in reconstructing dijet masses. Therefore, the choice $M_{\pi_T} = 160\,\text{GeV}$ reconstructs close to 150 GeV. *If* technipions decay mainly to light quarks and leptons, a plausible possibility for the lightest π_T, then we would expect all our input technihadron masses to decrease by 10–15 GeV.

[4] About 70% of the $W\pi_T$ rate at the LHC is due to the ρ_T.

[5] This includes $B(\pi_T \to \bar{q}q) \simeq 90\%$ in the default PYTHIA π_T-decay table.

cuts intended to enhance the π_T signal's significance and to make $\rho_T \to Wjj$ visible. Several distributions of data in the excess region $115\,\mathrm{GeV} < M_{jj} < 175\,\mathrm{GeV}$ published by CDF [2] — notably M_{Wjj}, $p_T(jj)$, $\Delta\phi$ and $\Delta R = \sqrt{(\Delta\eta)^2 + (\Delta\phi)^2}$ — fit the expectations of the LSTC model very well. The background-subtracted ΔR distribution, in particular, has a behavior which, we believe, furnishes strong support for our dijet production mechanism.

The purpose of this paper is to propose and study ways to test for the CDF signal at the LHC. In Sec. 2 we review the kinematics of $\rho_T, a_T \to W\pi_T$ and $Z\pi_T$ in LSTC. We also present an interesting new result: the nonanalytic behavior of $d\sigma/d(\Delta R)$ and $d\sigma/d(\Delta\chi)$ at their thresholds, $(\Delta R)_{\rm min}$ and $(\Delta\chi)_{\rm min}$. Here $\Delta\chi$ is the opening angle between the π_T decay jets in the ρ_T rest frame. For massless jets, a good approximation, we find that $(\Delta R)_{\rm min} = (\Delta\chi)_{\rm min} = 2\cos^{-1}(v)$, where $v = p_{\pi_T}/E_{\pi_T}$ is the π_T velocity in the ρ_T rest frame. This result, peculiar to production models such as LSTC in which a narrow resonance decays to another narrow resonance plus a W or Z, provides measures of v independent of p/E and, hence, valuable corroboration of this type of production. In Sec. 3 we consider the $\rho_T, a_T \to W\pi_T$ process. Its LHC cross section at 8 TeV is 9.5 pb but, for CDF cuts, its backgrounds have increased by about a factor of ten over those at the Tevatron. This makes testing for the dijet excess in this channel very challenging. We suggest cuts which enhance signal-to-background (S/B) but which will still require a very good understanding of the backgrounds in Wjj production. Recent studies of Wjj production by ATLAS and CMS are discussed there. In Sec. 4 we study $\rho_T^\pm, a_T^\pm \to Z\pi_T^\pm$, whose cross section is 2.8 pb at 8 TeV (190 fb after $Z \to e^+e^-$, $\mu^+\mu^-$). This is the isospin partner of $\rho_T^\pm, a_T^\pm \to W\pi_T^0$, so its cross section is rather confidently known. The $\ell^+\ell^-jj$ channel is free of QCD multijet and $\bar{t}t$ backgrounds and missing energy uncertainty. Reconstructing the Zjj invariant mass and other signal distributions, particularly in ΔR and $\Delta\chi$, will benefit from this. *Because of these features, we believe that the $Z\pi_T \to Zjj$ mode will be the surest test of CDF's dijet signal at the LHC.* In Sec. 5, we study $\rho_T^\pm, a_T^\pm \to WZ$. The cross section for this mode is proportional to $\tan^2\chi$ times the $\rho_T^\pm, a_T^\pm \to W^\pm\pi_T^0$ and $Z\pi_T^\pm$ rates, but enhanced by its greater phase space. We predict $\sigma(\rho_T^\pm, a_T^\pm \to WZ) = 1.8\ \ (1.1)$ pb for $\sin\chi = 1/3\,(1/4)$. In the all-leptons $3\ell\nu$ mode with e's and μ's, the rate is only 26 (15) fb, but jet-related uncertainties are absent except insofar as they effect $\not{E}_T$ resolution. A new study by CMS of this channel is discussed there. The $WZ \to \ell^+\ell^-jj$ mode is also an interesting target of opportunity so long as $\sin\chi \gtrsim 1/4$. The ΔR and $\Delta\chi$ distributions for $Z \to jj$ again provide support for our narrow LSTC-resonance production model. In short, one or both of the $Z\pi_T$ and WZ modes should be dispositive of the LSTC interpretation of the CDF dijet excess with the $\sim 20\,\mathrm{fb}^{-1}$ expected by the end of 2012. We present in an appendix the details of calculations in Sec. 2 regarding the nonanalytic threshold behavior of the $\Delta\chi$ and ΔR distributions.

While the simulations of the CDF signal in this paper are made in the context of low-scale technicolor, their qualitative features apply to any model in which that signal is due to $\bar{q}q$ production of a narrow resonance decaying to a W plus another narrow resonance. Several papers have appeared proposing such an s-channel mechanism [22, 23, 24, 25, 26, 27]. With similar resonance masses to our LSTC proposal, these models will have kinematic

distributions like those we describe in Sec. 2. However, not all these models will have the Zjj and WZ signals of LSTC. There are also a large number of papers proposing that the CDF signal is due to production of a new particle (e.g., a leptophobic Z') that is not resonantly produced [28, 29, 30, 31, 32, 33, 34]. These "t-channel" models will not pass our kinematic tests.

2. LSTC Kinematics and Threshold Nonanalyticity

The kinematics of $\rho_T \to W\pi_T$ at the Tevatron and LHC are a consequence of the basic LSTC feature that walking TC enhancements of M_{π_T} strongly suggest $M_{\rho_T} < 2M_{\pi_T}$ and, indeed, that the phase space for $\rho_T \to W\pi_T$ is quite limited [13, 35]. At the Tevatron, a 290 GeV ρ_T is produced almost at rest, with almost no p_T and very little boost along the beam direction. At the LHC, $p_T(\rho_T) \lesssim 25\,\text{GeV}$ and $\eta(\rho_T) \lesssim 2.0$. Furthermore, the π_T is emitted very slowly in the ρ_T rest frame — $v \simeq 0.4$ for our assumed masses — so that its decay jets are roughly back-to-back in the lab frame. Thus, $p_T(\pi_T) \lesssim 80\,\text{GeV}$ and the z-boost invariant quantities $\Delta\phi$ and $\Delta R = \sqrt{(\Delta\eta)^2 + (\Delta\phi)^2}$ are peaked at large values less than π.

These features of LSTC are supported by CDF's $7.3\,\text{fb}^{-1}$ data [2]. Figures 1–4 show distributions before and after background subtraction taken from the $115 < M_{jj} < 175\,\text{GeV}$ region containing the dijet excess. The subtracted-data M_{Wjj} signal has a narrow resonant shape quite near 290 GeV. Unfortunately, the background peaks not far below that mass so that one may be concerned that the subtracted data's peak is due to underestimating the background. Also, as we expect, the subtracted $p_T(jj)$ data falls off sharply above 75 GeV and the subtracted $\Delta\phi$ data is strongly peaked at large values. Again, one may worry that these are artifacts of the peak of the M_{Wjj} background and the position of the M_{jj} excess.

The background-subtracted ΔR distribution, however, is very interesting. It is practically zero for $\Delta R < 2.25$, then rises sharply to a broad maximum before falling to zero again at $\Delta R \simeq 3.5$. This behavior, and a somewhat similar one we predict for $\Delta\chi$ are the main subject of this section. We will show that the threshold form of the ΔR and $\Delta\chi$ distributions provide direct measures of the velocity of the dijet system in the subprocess center-of-mass frame that are independent of measuring p/E and, thus, are independent checks on the two-resonance topology of the dijet's production mechanism.[6] One might think that the corresponding $\Delta R_{\ell\ell}$ and $\Delta\chi_{\ell\ell}$ distributions from $Z \to \ell^+\ell^-$ would be similarly valuable. Unfortunately, because the dileptons come from real Z's and our cuts make the background Z's like the signal ones, $\Delta R_{\ell\ell}$ and $\Delta\chi_{\ell\ell}$ are indistinguishable from their backgrounds.

For our analysis, we assume the jets from π_T decay are massless. We have examined the effect of including jet masses and found them to be unimportant. We will remark briefly on this at the end of this section. We first consider the dominant ρ_T contribution to $W/Z\pi_T$

[6]Note that ΔR and $\Delta\chi$ are largely unaffected by lost neutrinos if semileptonic b-decays are an important component of π_T decays. Also, $\Delta\chi$ is defined in the ρ_T rest frame, while ΔR is defined in the lab frame. If one wishes to remove the effect of $p_T(\rho_T)$ on ΔR, it should be defined in the ρ_T frame.

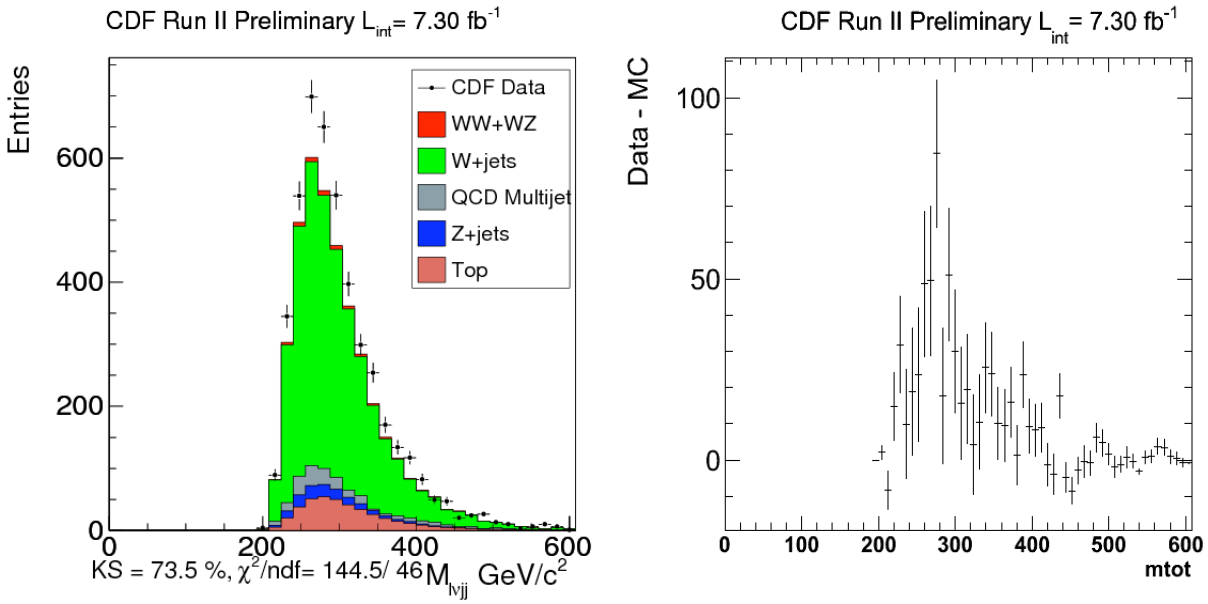

Figure 1: CDF M_{Wjj} distributions for $\int \mathcal{L}dt = 7.3\,\mathrm{fb}^{-1}$ from the dijet signal region $115 < M_{jj} < 175\,\mathrm{GeV}$ [2]. Left: Expected backgrounds and data; right: background subtracted data.

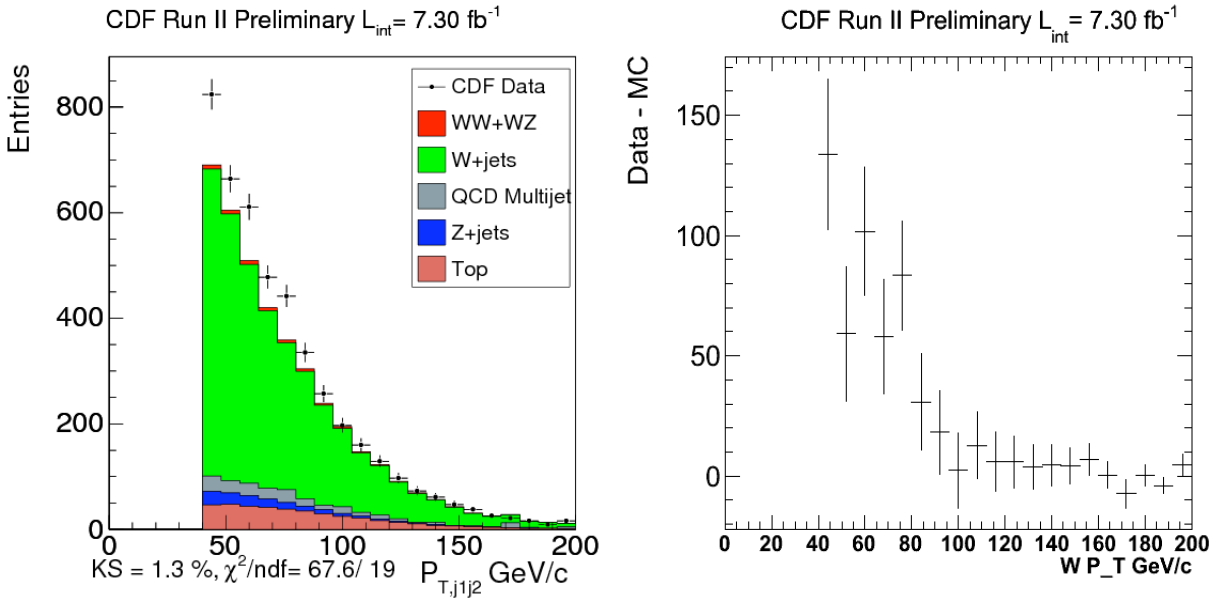

Figure 2: CDF $p_T(jj)$ distributions for $\int \mathcal{L}dt = 7.3\,\mathrm{fb}^{-1}$ from the dijet signal region $115 < M_{jj} < 175\,\mathrm{GeV}$ [2]. Left: Expected backgrounds and data; right: background subtracted data.

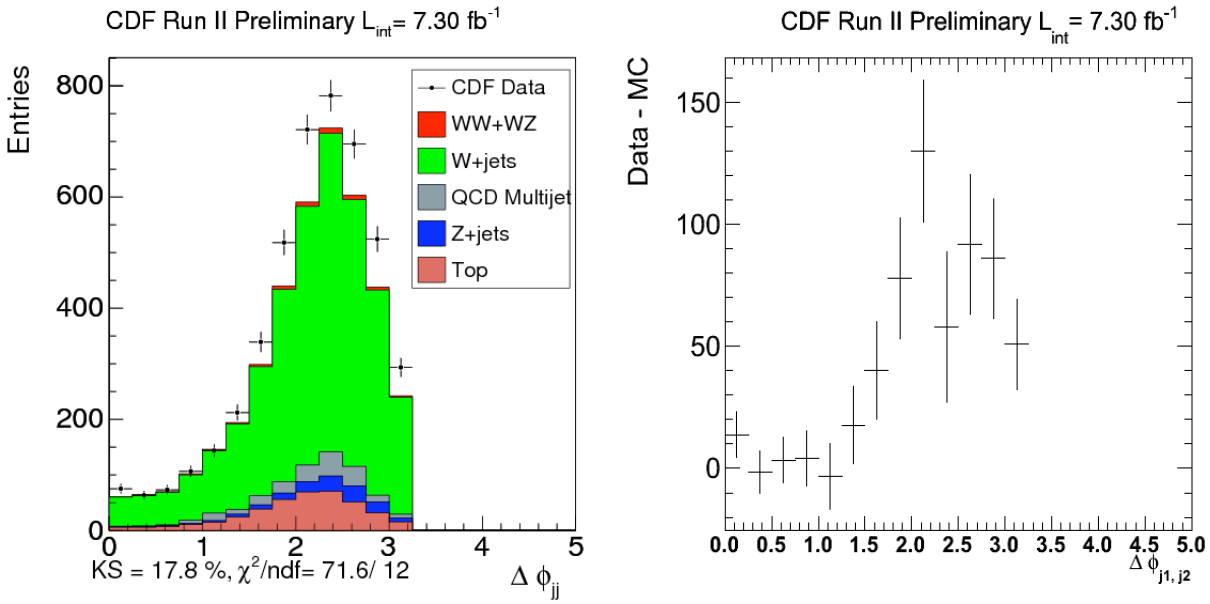

Figure 3: CDF $\Delta\phi$ distributions for $\int \mathcal{L}dt = 7.3\,\mathrm{fb}^{-1}$ from the dijet signal region $115 < M_{jj} < 175\,\mathrm{GeV}$ [2]. Left: Expected backgrounds and data; right: background subtracted data.

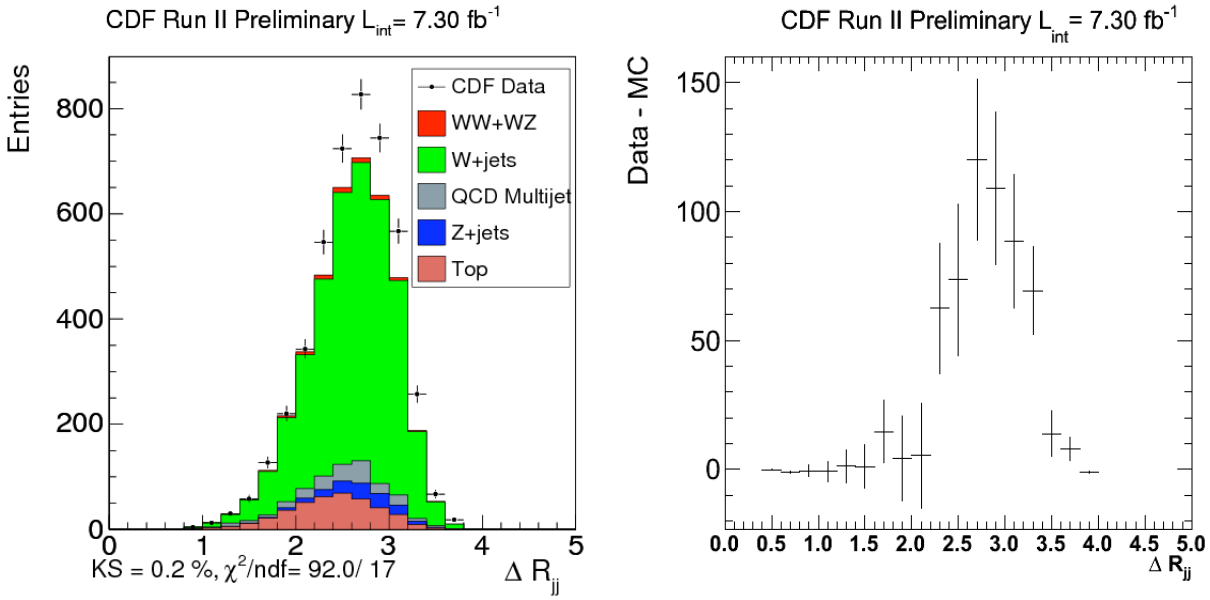

Figure 4: CDF ΔR distributions for $\int \mathcal{L}dt = 7.3\,\mathrm{fb}^{-1}$ from the dijet signal region $115 < M_{jj} < 175\,\mathrm{GeV}$ [2]. Left: Expected backgrounds and data; right: background subtracted data.

production, commenting on the a_T contribution also at the end.

Define the angles θ, θ^* and ϕ^* as follows: Choose the z-axis as the direction of the event's boost; this is usually the direction of the incoming quark in the subprocess c.m. frame. In the ρ_T rest frame, θ is the polar angle of the π_T velocity $\boldsymbol{v}$, the angle it makes with the z-axis. Define the xz-plane as the one containing the unit vectors $\hat{\boldsymbol{z}}$ and $\hat{\boldsymbol{v}}$, so that $\hat{\boldsymbol{v}} = \hat{\boldsymbol{x}}\sin\theta + \hat{\boldsymbol{z}}\cos\theta$, and $\hat{\boldsymbol{y}} = \hat{\boldsymbol{z}} \times \hat{\boldsymbol{x}}$. Define a starred coordinate system *in the π_T rest frame* by making a rotation by angle θ about the y-axis of the ρ_T frame. This rotation takes $\hat{\boldsymbol{z}}$ into $\hat{\boldsymbol{z}}^* = \hat{\boldsymbol{v}}$ and $\hat{\boldsymbol{x}}$ into $\hat{\boldsymbol{x}}^* = \hat{\boldsymbol{x}}\cos\theta - \hat{\boldsymbol{z}}\sin\theta$. In this frame, let $\hat{\boldsymbol{p}}_1^*$ be the unit vector in the direction one of the jets (partons). The angle between $\hat{\boldsymbol{v}}$ and $\hat{\boldsymbol{p}}_1^*$ is θ^*; the azimuthal angle of $\boldsymbol{p}_1^* = -\boldsymbol{p}_2^*$ is ϕ^*:

$$\cos\theta = \hat{\boldsymbol{z}} \cdot \hat{\boldsymbol{v}}, \quad \cos\theta^* = \hat{\boldsymbol{p}}_1^* \cdot \hat{\boldsymbol{v}}, \quad \tan\phi^* = p_{1y^*}^*/p_{1x^*}^*. \tag{1}$$

Note that, since $\pi_T \to \bar{q}q$ is isotropic in its rest frame, $d\sigma(\bar{q}q \to \rho_T \to Wjj)/d(\cos\theta^*) = \sigma/2$, where σ is the total subprocess cross section.

It is easier to consider the $d\sigma/d(\Delta\chi)$ distribution first. For massless jets,

$$1 - \cos(\Delta\chi) = \frac{2(1-v^2)}{1 - v^2\cos^2\theta^*}\,. \tag{2}$$

The minimum value of $\Delta\chi$ occurs when $\theta^* = \pi/2$ (i.e., $\boldsymbol{v} \perp \boldsymbol{p}_1^*$), and so

$$\pi \geq \Delta\chi \geq (\Delta\chi)_{\min} = 2\cos^{-1}(v)\,. \tag{3}$$

From Eq. (2), it is easy to see that

$$\frac{d\sigma}{d(\Delta\chi)} = \frac{(1-v^2)\,\sigma}{4v\sin^2(\Delta\chi/2)\sqrt{\cos^2((\Delta\chi)_{\min}/2) - \cos^2((\Delta\chi)/2)}}\,. \tag{4}$$

The $\Delta\chi$ distribution has an inverse-square-root singularity at $\Delta\chi = (\Delta\chi)_{\min} = 2\cos^{-1}(v) = 2.23$ for our input masses, and falls sharply above there. This is illustrated in Fig. 5 where we plot this distribution for the primary partons and for the reconstructed jets. The low-side tail for the jets is an artifact of their reconstruction.

To understand this singularity better, it follows from Eq. (2) that $\Delta\chi$ may be expanded about $\cos\theta^* = 0$ as

$$\Delta\chi = (\Delta\chi)_{\min} + \frac{a}{2}\cos^2\theta^* \ + \cdots\,, \tag{5}$$

where a is a positive v-dependent coefficient. Then, near $\cos\theta^* = 0$, i.e., the $\Delta\chi$ threshold,

$$\frac{d\sigma}{d(\Delta\chi)} = \frac{\sigma}{2}\,\frac{d(\cos\theta^*)}{d(\Delta\chi)} \propto \frac{1}{\sqrt{\Delta\chi - (\Delta\chi)_{\min}}}\,. \tag{6}$$

It is the simple one-variable Taylor expansion of $\Delta\chi$ in Eq. (5) that has caused this singularity.

The discussion of $d\sigma/d(\Delta R)$ for the LSTC signal shares some features with $d\sigma/d(\Delta\chi)$, though it it is qualitatively different. The ΔR distribution also vanishes below a threshold,

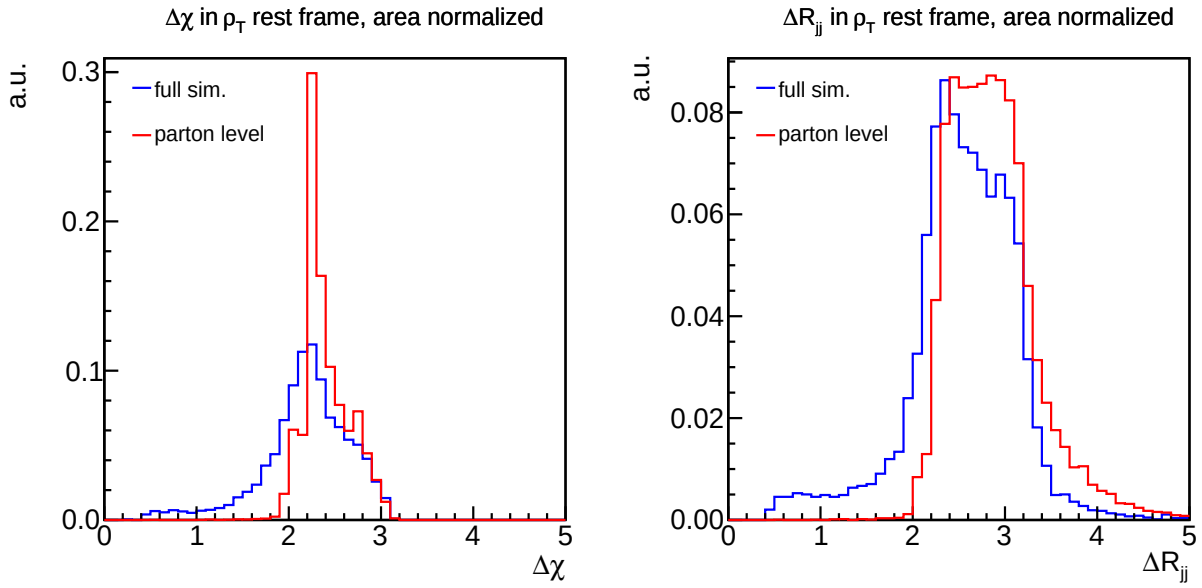

Figure 5: The area-normalized $\Delta\chi$ and ΔR distributions for the primary parton/jet in $\rho_T, a_T \to W\pi_T$ production followed by $\pi_T \to \bar{q}q$ decay, constructed as described in the text. Red: pure distribution of primary parton before any radiation; blue: the distribution for the jets reconstructed as described in Sec. 3.

$(\Delta R)_{\rm min}$, which is equal to $(\Delta\chi)_{\rm min} = 2\cos^{-1}(v)$. This remarkable feature, derived in the appendix, can be understood simply as a consequence of the fact that the minimum of ΔR occurs when *both* jet rapidities vanish. In that case, $\Delta R = \Delta\phi = \Delta\chi$.

At threshold, however, the ΔR distribution is $\propto \sqrt{\Delta R - (\Delta\chi)_{\rm min}}$, not the inverse square root. As illustrated in Fig. 5, it rises sharply from threshold into a broad feature before decreasing. The measure of the π_T velocity v is given by the onset of the rise, not its peak. This is the behavior seen in the CDF data in Fig. 4, where the rise starts very near $2\cos^{-1}(v) = 2.23$ for our input masses. Both the $\Delta\chi$ and ΔR distributions measure the π_T velocity v and, therefore, provide confirmations of the $\rho_T \to W\pi_T$ hypothesis which are *independent* of the background under the M_{Wjj} resonant peak and of uncertainty in the $\not{E}_T$ resolution as well.

The reason for this qualitative difference between the two distributions is that $d\sigma/\Delta\chi$ involves a one-dimensional trade of $\cos\theta^*$ for $\Delta\chi$, whereas ΔR is parametrized in terms of the three angles θ, θ^*, ϕ^* in an intricate way, with all three being integrated over to account for the constraint defining ΔR. In contrast to what happens in the $\Delta\chi$ case, the Jacobian singularity at the threshold is "antidifferentiated" twice, hence its comparatively lower strength. Using a Fadeev-Popov-like trick, the ΔR distribution can be written

$$\frac{d\sigma}{d(\Delta R)} = \int d(\cos\theta)\, d(\cos\theta^*) d(\cos\phi^*)\, \frac{d\sigma}{d(\cos\theta^*)}\, \delta\left(\Delta R - f(\cos\theta, \cos\theta^*, \cos\phi^*)\right) . \qquad (7)$$

The function $f(\cos\theta, \cos\theta^*, \cos\phi^*)$ is shown in the appendix to have its absolute minimum at $\cos\theta = \cos\theta^* = \cos\phi^* = 0$, for which its value is equal to $(\Delta\chi)_{\rm min}$. Near its minimum it is locally parabolic and its Taylor expansion is

$$f(\cos\theta, \cos\theta^*, \cos\phi^*) = (\Delta\chi)_{\rm min} + \tfrac{1}{2}\left(b_\theta \cos^2\theta + b_{\theta^*}\cos^2\theta^* + b_{\phi^*}\cos^2\phi^*\right) + \cdots \qquad (8)$$

The positive v-dependent coefficients b_θ, b_{θ^*} and b_{ϕ^*} are also given in the appendix, Eq. (29). For ΔR close to $(\Delta\chi)_{\rm min}$, this expansion can be used to approximate Eq. (7). In a similar way as for the $\Delta\chi$ distribution, integrating first over $\cos\theta^*$ generates the appearance of a Jacobian inverse square root singularity $\propto [2(\Delta R - (\Delta\chi)_{\rm min}) - (b_\theta\cos^2\theta + b_{\phi^*}\cos^2\phi^*)]^{-1/2}$. The two remaining integrations over $\cos\theta$ and $\cos\phi^*$ were trivial in the $\Delta\chi$ case as the integrand did not depend on them, but this is not so for ΔR which involves a double integration over a restricted angular phase space defined by

$$0 \le b_\theta\cos^2\theta + b_{\phi^*}\cos^2\phi^* \le 2\,(\Delta R - (\Delta\chi)_{\rm min})\ . \qquad (9)$$

Performing the integral in Eq. (7) near $(\Delta R)_{\rm min} = (\Delta\chi)_{\rm min}$ yields a result $\propto \sqrt{\Delta R - (\Delta\chi)_{\rm min}}$.

We have examined the effect of finite jet masses (as opposed to jet reconstruction and energy resolution) on the threshold values of the ΔR and $\Delta\chi$ distributions and the extraction of the π_T velocity v from them. Our jets (which include b-jets in the Pythia default π_T-decay table) have masses $\lesssim 10\,\text{GeV}$. Assuming, for simplicity, equal jet masses and denoting by $u = \sqrt{1 - 4M_{\rm jet}^2/M_{\pi_T}^2}$ the jet velocity in the π_T rest frame, the corrected $(\Delta\chi)_{\rm min}(u)$ is

$$(\Delta\chi)_{\rm min}(u) = \cos^{-1}\frac{v^2 - u^2(1-v^2)}{v^2 + u^2(1-v^2)} \simeq \cos^{-1}(2v^2-1) - v(1-v^2)^{1/2}(1-u^2)\,. \qquad (10)$$

This is less than the massless $(\Delta\chi)_{\rm min}$ by half a percent for $M_{\rm jet} = 10\,\text{GeV}$.

Finally, as noted, the a_T accounts for about 25–30% of $W\pi_T$ production. This decay gives a π_T velocity of 0.54 in the a_T rest frame and $(\Delta\chi)_{\rm min} = 2.00$. The effect is clearly visible in the $\Delta\chi$ and ΔR distributions for the primary parton in Fig. 5, but is washed out by the low-end tails for the reconstructed jets. We believe that the low and high-end tails are due to the two π_T jets fragmenting to three jets and the two leading jets being closer or farther apart than the original pair. It turns out that our Q-value cut for $Z\pi_T$ in Sec. 4 eliminates the a_T contribution to the signal.

3. The $\rho_T, a_T \to W\pi_T$ mode at the LHC

As a reminder, we assumed $M_{\rho_T} = 290\,\text{GeV}$, $M_{a_T} = 1.1M_{\rho_T} = 320\,\text{GeV}$, $M_{\pi_T} = 160\,\text{GeV}$ and $\sin\chi = 1/3$ to describe the CDF dijet excess. The Tevatron cross section is 2.2 pb. At the 8 TeV LHC, these parameters give $\sigma(W\pi_T) = 9.5\,\text{pb}$ (2.0 pb for $W \to e\nu,\ \mu\nu$). These cross sections are 20% higher than at 7 TeV, but this does not translate into a 20% increase in S/B. About 70% of the LHC rate is due to the ρ_T; the ρ_T and a_T interference is very

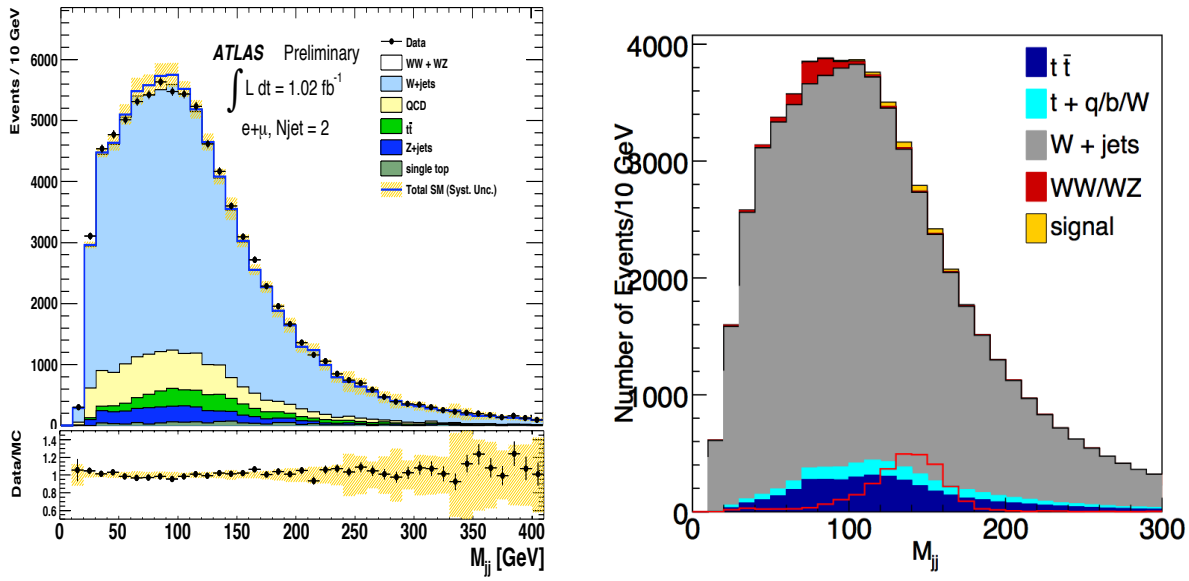

Figure 6: Left: The ATLAS M_{jj} distribution for exactly two jets in Wjj production at $\sqrt{s} = 7\,\text{TeV}$ and $\int \mathcal{L}dt = 1.02\,\text{fb}^{-1}$; from Ref. [36] Right: Simulation of the M_{jj} distribution in Wjj production with ATLAS cuts (except that $p_T(\ell) > 30\,\text{GeV}$) for $1.0\,\text{fb}^{-1}$. The open red histogram is the $\pi_T \to jj$ signal *times 10*.

small. For such close masses, it is impossible to resolve the two resonances in the M_{Wjj} spectrum.

Last summer, the ATLAS Collaboration published dijet spectra for $1.02\,\text{fb}^{-1}$ of Wjj data with exactly two jets and with two or more jets passing selection criteria [36]. The ATLAS cuts, taken as close to CDF's as practical, were: one isolated electron with $E_T > 25\,\text{GeV}$ or muon with $p_T > 20\,\text{GeV}$ and rapidity $|\eta_\ell| < 2.5$; $\not\!\!E_T > 25\,\text{GeV}$ and $M_T(W) > 40\,\text{GeV}$; two (or more) jets with $p_T > 30\,\text{GeV}$ and $|\eta_j| < 2.8$; and $p_T(jj) > 40\,\text{GeV}$ and $\Delta\eta < 2.5$ for the two leading jets. The M_{jj} distribution for the two-jet data is shown in Fig. 6. There is no evidence of CDF's dijet excess near 150 GeV nor even of the standard model WW/WZ signal near 80 GeV. This is what we anticipated in Ref. [6] because of the great increase in Wjj backgrounds at the LHC relative to the Tevatron. On the other hand, it is noteworthy and encouraging for future prospects that the ATLAS background simulation appears to fit the data well.

In Fig. 6 we also show our simulation of the LSTC M_{jj} signal and backgrounds at the LHC for $\sqrt{s} = 7\,\text{TeV}$ and $\int \mathcal{L}dt = 1.0\,\text{fb}^{-1}$. ATLAS's cuts were used except that we required $p_T(\ell) > 30\,\text{GeV}$.[7] This tighter cut and our inability to include the data-driven

[7]Backgrounds were generated at matrix-element level using ALPGENv213 [37], then passed to PYTHIAv6.4 for showering and hadronization. We use CTEQ6L1 parton distribution functions and a factorization/renormalization scale of $\mu = 2M_W$ throughout. For the dominant W+jets background we generate $W + 2j$ (exclusive) plus $W + 3j$ (inclusive) samples, matched using the MLM procedure [38] (parton level

QCD background account for our lower event rate compared to ATLAS. Despite this, the agreement between the two is quite good. In particular, our simulation shows that the CDF/ATLAS cuts can neither reveal nor exclude the LSTC interpretation of the CDF signal at the LHC for any reasonable luminosity.[8]

Recently, the CMS Collaboration studied the dijet-mass spectrum in $W(\to \ell\nu)$ plus jets production with $4.7\,\text{fb}^{-1}$ at 7 TeV [43, 44]. CMS used the following cuts which were partly adopted from Ref. [7]: $p_T(e,\mu) > 25, 30\,\text{GeV}$ and rapidity $|\eta(e,\mu)| < 2.5, 2.1$, $\Delta R(\ell, j) > 0.3$; $\not\!\!E_T(e,\mu) > 35, 25\,\text{GeV}$, $\Delta\phi(\not\!\!E_T, j) > 0.4$; $M_T(W) > 50\,\text{GeV}$ and $p_T(W) > 60\,\text{GeV}$; exactly two or three jets with $p_{T1} > 40\,\text{GeV}$, $p_{T2,3} > 30\,\text{GeV}$, $|\eta_j| < 2.4$; and $p_T(jj) > 45\,\text{GeV}$, $\Delta\eta(jj) < 1.2$. CMS used MadGraph to generate W + jets and a data-driven method to determine the M_{jj} shape and background: A superposition of a set of templates was constructed in which the MadGraph factorization and renormalization scales were varied up and down by a factor of two from their default values, and this was fit to the dijet spectrum *outside* the signal region, taken to be 123 to 186 GeV. The Wjj background in the signal region was then determined from this fit. The CMS dijet spectra before and after background subtraction are shown in Fig. 7. Note that the vertical scale is "Events/GeV." No significant enhancement near 150 GeV was observed. (What CMS meant by a "CDF-like signal" is not specified in Ref. [43, 44].) Using a WH production model, CMS reported a 95% upper limit on the production cross section times $B(W \to \ell\nu)$ of 1.3 pb.

We studied the LSTC Wjj signal at $\sqrt{s} = 7\,\text{TeV}$ in Ref. [7], before the CMS paper's release. Our prediction for the cross section was $\sigma B = 1.7\,\text{pb}$, 30% higher than CMS's limit. In order to achieve a better outcome than ATLAS's 2011 study, we examined a variety of cuts motivated by $\rho_T \to W\pi_T$ kinematics. Cuts quite similar to those we proposed for the Tevatron in Ref. [5] typically caused the background to peak very near the dijet resonance. To get the signal off the peak (and more like the original CDF M_{jj} excess [1]), we used the following: lepton $p_{T\ell} > 30\,\text{GeV}$ and $|\eta_\ell| < 2.5$, $\not\!\!E_T > 25\,\text{GeV}$, $M_T(W) > 40\,\text{GeV}$ and $p_T(W) > 60\,\text{GeV}$; exactly two jets with $p_{T1} > 40\,\text{GeV}$, $p_{T2} > 30\,\text{GeV}$, $|\eta_j| < 2.8$; $p_T(jj) > 45\,\text{GeV}$, $\Delta\eta(jj) < 1.2$; and $Q = M_{Wjj} - M_{jj} - M_W < 100\,\text{GeV}$. The resulting M_{jj} distribution is also displayed in Fig. 7. Counting events in the range $120 < M_{jj} < 170\,\text{GeV}$ gives $S/\sqrt{B} = 6.5$ for this luminosity, but only $S/B = 0.050$. The ΔR and $\Delta\chi$ signals are also small and not useful. Because of the small S/B, and in view of the difficulty CMS had fitting the dijet spectrum in the diboson and CDF-signal region, we believe that a better

cuts are imposed to ensure that $W + 0, 1$ jet events cannot contribute). After matching, the overall normalization is scaled to the NLO $W + jj$ value, calculated with MCFMv6 [39]. After passing through Pythia, final state particles are combined into (η, ϕ) cells of size 0.1×0.1, and the energy in each cell smeared with $\Delta E/E = 1.0/\sqrt{E/\text{GeV}}$. The energy of each cell is rescaled to make it massless. Isolated photons and leptons (e, μ) are removed, and all remaining cells with energy greater than 1 GeV are clustered into jets using FastJet (anti-kT algorithm, $R = 0.4$) [40]. Estimates of the background including higher order effects have been shown to be completely consistent with our LO+PS treatment [41, 42]. Finally, the quadratic ambiguity in the W reconstruction was resolved by choosing the solution with the smaller $p_z(\nu)$.

[8] Models of the CDF signal that are gg-initiated or involve large coupling to heavier quarks, e.g., Refs. [27, 32], are likely excluded by the ATLAS data.

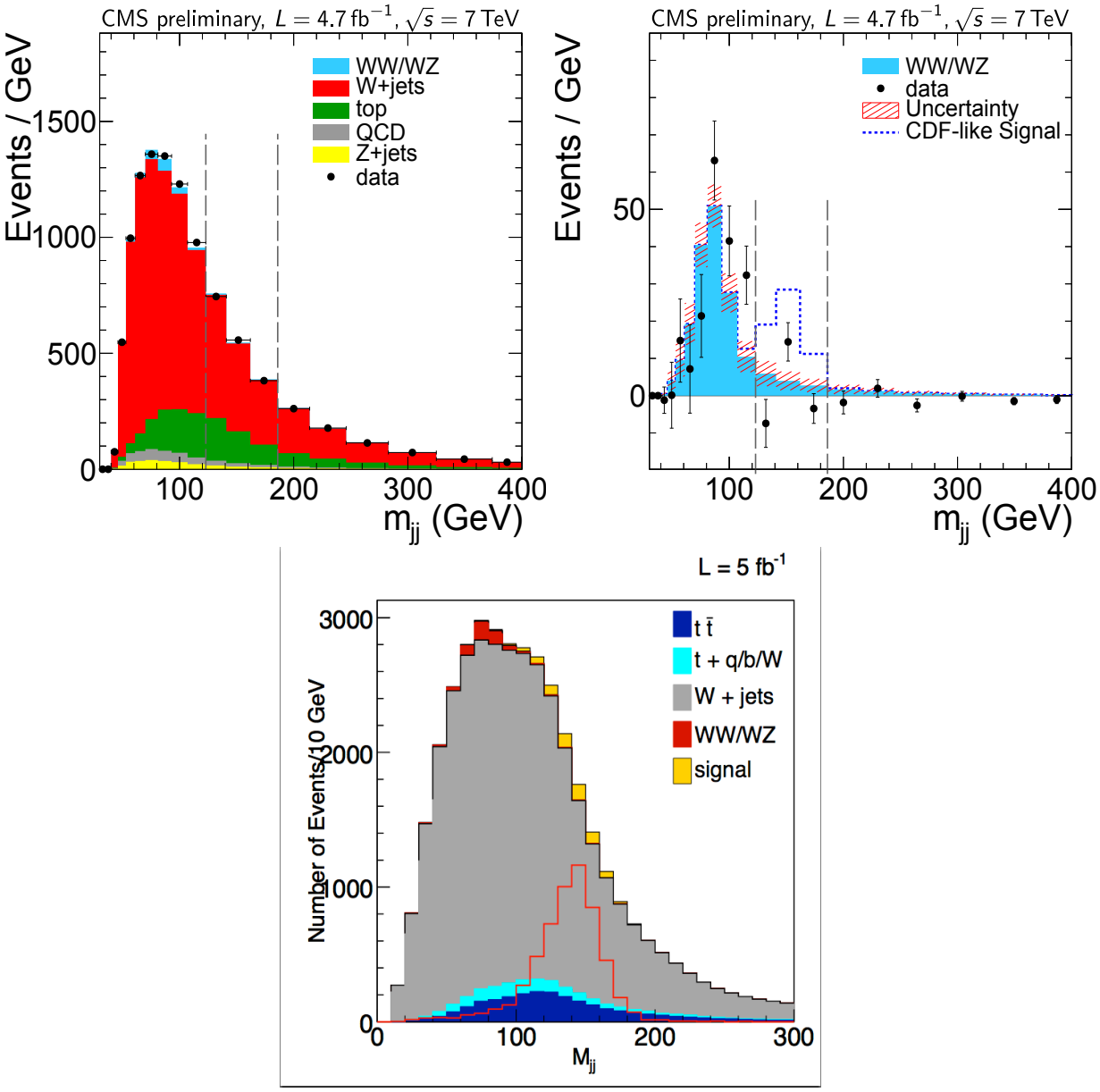

Figure 7: The CMS M_{jj} distributions for $4.7\,\mathrm{fb}^{-1}$ of $W \to \mu\nu$, $e\nu$ plus two or three jets data at $\sqrt{s} = 7\,\mathrm{TeV}$ before (top left) and after (top right) the background subtraction summarized in the text; from Ref. [43, 44]. On the bottom is our M_{jj} distribution for the $\rho_T, a_T \to W\pi_T \to \ell\nu_\ell jj$ signal and backgrounds at the LHC for $5\,\mathrm{fb}^{-1}$. Augmented ATLAS-like cuts as described in the text were used. The open red histograms are the π_T and ρ_T signals *times 10*.

understanding of the backgrounds is required to observe or exclude the LSTC signal in this channel.

Our simulations of the M_{jj} and M_{Wjj} distributions in Wjj production at $\sqrt{s} = 8\,\mathrm{TeV}$

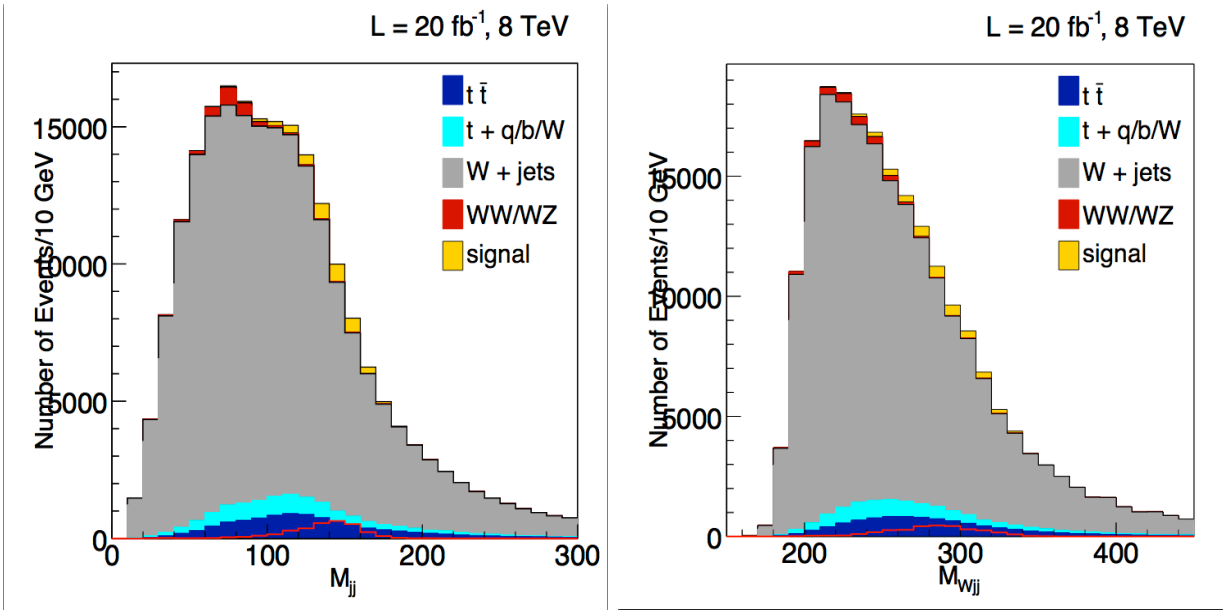

Figure 8: The M_{jj} and M_{Wjj} distributions of $\rho_T, a_T \to W\pi_T \to \ell\nu_\ell jj$ and backgrounds at the LHC for $\sqrt{s} = 8\,\text{TeV}$ and $\int \mathcal{L}dt = 20\,\text{fb}^{-1}$. Augmented ATLAS-like cuts as described in the text are employed. The open red histograms are the unscaled π_T and ρ_T signals.

are shown in Fig. 8 for $\int \mathcal{L}dt = 20\,\text{fb}^{-1}$. The same cuts as above are used. Counting events in the range $120 < M_{jj} < 170\,\text{GeV}$ gives $S/\sqrt{B} = 10.2$ for this luminosity but still only $S/B = 0.050$. Despite this large "significance", we are chary of the ability of the $\ell\nu jj$ channel to settle the questions of CDF's dijet excess and our interpretation of it.

4. The $\rho_T^\pm, a_T^\pm \to Z\pi_T^\pm$ mode

In view of this situation with the $W\pi_T$ signal, observation of the isospin partner $\rho_T^\pm, a_T^\pm \to Z\pi_T^\pm$ of the $W\pi_T^0$ mode can provide the needed test of the LSTC interpretation of CDF's Wjj signal. At the LHC, we predict $\sigma(\rho_T^\pm, a_T^\pm \to Z\pi_T^\pm) = 2.8\,\text{pb}$, lower than $\sigma(\rho_T^\pm, a_T^\pm \to W\pi_T^0) = 4.1\,\text{pb}$ because of the reduced phase space, $\propto p^3$. Then, $\sigma(\rho_T^\pm, a_T^\pm \to Z\pi_T \to \ell^+\ell^- jj) = 190\,\text{fb}$ for $\ell = e$ and μ, of which, 80% is due to the $\rho_T^\pm$. This rate is about 10% of the $W\pi_T \to \ell\nu_\ell jj$ signal. We might expect, therefore, that ~ 10 times the luminosity needed for the $W\pi_T$ signal would be required for the same sensitivity to $Z\pi_T$. Actually, the situation is better than this because there is no QCD multijet background nor $\not{E}_T$ resolution to pollute the Zjj data.

Figure 9 shows the $Z\pi_T$ signal and its background, almost entirely from Z + jets, for $\sqrt{s} = 8\,\text{TeV}$ and $\int \mathcal{L}dt = 20\,\text{fb}^{-1}$. The cuts used here are: two electrons or muons of opposite charge with $p_T > 30\,\text{GeV}$, $|\eta_\ell| < 2.5$, $80 < M_{\ell^+\ell^-} < 100\,\text{GeV}$ and $p_T(Z) > 50\,\text{GeV}$; exactly two jets with $p_T > 30\,\text{GeV}$ and $|\eta_j| < 2.8$; $p_T(jj) > 40\,\text{GeV}$, $\Delta\eta(jj) < 1.75$; and

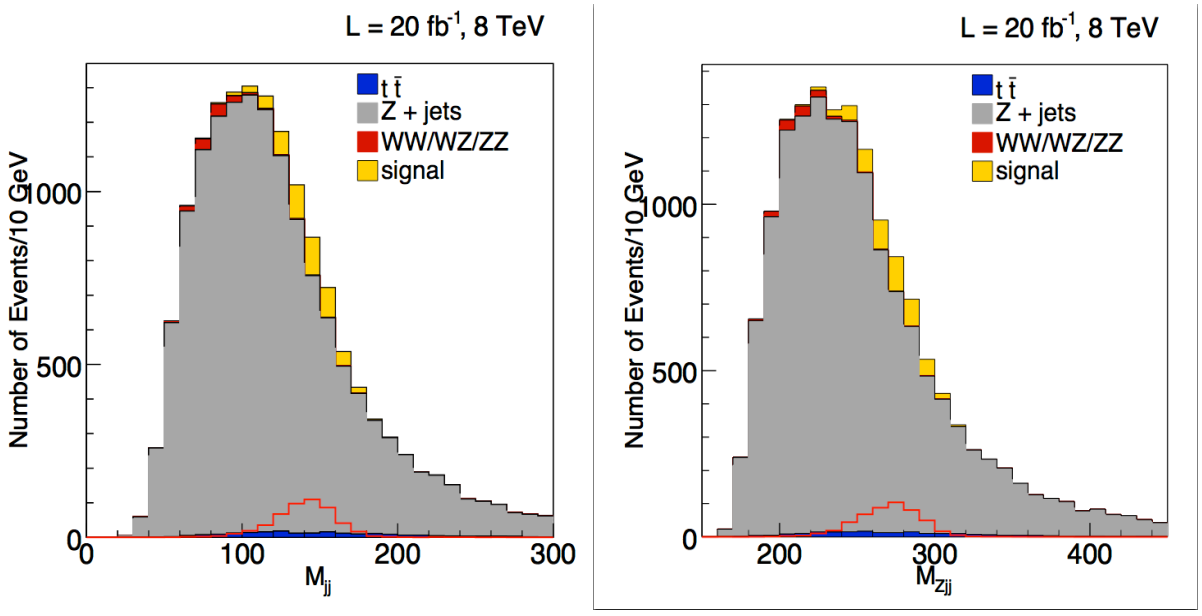

Figure 9: The M_{jj} and M_{Zjj} distributions of $\rho_T^\pm \to Z\pi_T^\pm \to \ell^+\ell^- jj$ and backgrounds at the LHC for $\sqrt{s} = 8\,\text{TeV}$ and $\int \mathcal{L}dt = 20\,\text{fb}^{-1}$. The cuts used are described in the text. The open red histograms are the π_T and ρ_T signals.

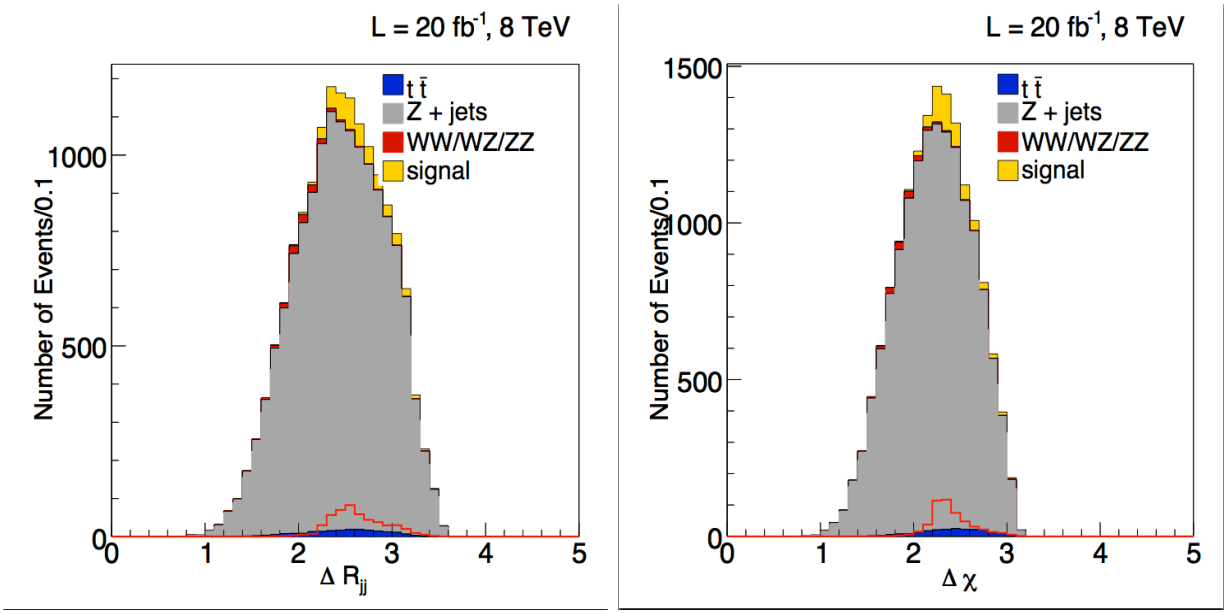

Figure 10: The ΔR and $\Delta\chi$ distributions for $\rho_T^\pm \to Z\pi_T^\pm \to \ell^+\ell^- jj$ and backgrounds at the LHC for $\sqrt{s} = 8\,\text{TeV}$ and $\int \mathcal{L}dt = 20\,\text{fb}^{-1}$. The cuts used are described in the text. The open red histograms are the signals.

$Q = M_{Zjj} - M_{jj} - M_Z < 60\,\text{GeV}$. This Q-cut is very important in reducing the background. However, it excludes the 20% of $Z\pi_T$ that comes from $a_T^\pm$ production.[9] These give $S/\sqrt{B} = 6.2$ and $S/B = 0.11$ for the dijet signal in $120 < M_{jj} < 170\,\text{GeV}$. The figure also shows the M_{Zjj} distribution; it has $S/\sqrt{B} = 6.4$ and $S/B = 0.12$ for $250 < M_{Zjj} < 320\,\text{GeV}$. These signal-to-background rates and the position of the dijet signal on the falling backgrounds are similar to those in Ref. [2]. Therefore, if our interpretation of the CDF dijet excess is correct, both $\pi_T \to jj$ and $\rho_T \to \ell^+\ell^- jj$ will be observable soon.

Figure 10 shows the ΔR and $\Delta\chi$ distributions for $\rho_T \to Z\pi_T \to \ell^+\ell^- jj$. The skyscraper-shaped $\Delta\chi$ distribution is especially interesting. The background peaks at $\Delta\chi \simeq 2.3$, and appears rather symmetrical about this point except that its high side falls more rapidly above 2.7 because $(\Delta\chi)_{\max} = \pi$. The signal's $\Delta\chi$ distribution sits atop the skyscraper, concentrated in about 330 events in three bins at $\Delta\chi = 2.2$–2.4, whereas the theoretical $(\Delta\chi)_{\min} = 2\cos^{-1}(v) = 2.31$ for $\rho_T \to Z\pi_T$. This is just as expected when jet reconstruction is taken into account; see Fig. 5. If the actual $\Delta\chi$ data, with our cuts, has the shape of our simulation, we believe the signal excess can be observed. Similar remarks apply to the shape and observability of the slightly broader ΔR distribution in Fig. 10.

5. The $\rho_T^\pm, a_T^\pm \to WZ$ mode

Finally, the decay channel $\rho_T^\pm, a_T^\pm \to W^\pm Z$ furnishes another important check on the LSTC hypothesis provided that $\sin\chi \gtrsim 1/4$. The dominant contribution, $\rho_T \to W_L Z_L$, has an angular distribution $\propto \sin^2\theta$ so that the production is fairly central. We expect $\sigma(\rho_T, a_T \to WZ)/\sigma(\rho_T, a_T \to W\pi_T^0) \simeq (p(Z)/p(\pi_T))^3 \tan^2\chi$. The PYTHIA rates are roughly consistent with this. For our input masses and $\sin\chi = (\frac{1}{5}, \frac{1}{4}, \frac{1}{3}, \frac{1}{2})$, we obtain the following cross sections:

$$\sigma(\rho_T, a_T \to WZ \to \ell^+\ell^-\ell^\pm\nu_\ell) = (9,\ 15,\ 26,\ 54)\,\text{fb}\,, \tag{11}$$

$$\sigma(\rho_T, a_T \to WZ \to \ell^+\ell^- jj) = (27,\ 48,\ 80,\ 170)\,\text{fb}\,, \tag{12}$$

$$\sigma(\rho_T, a_T \to WZ \to \ell\nu jj) = (90,\ 155,\ 260,\ 555)\,\text{fb}\,, \tag{13}$$

$$\sigma(\rho_T, a_T \to WW \to \ell\nu jj) = (140,\ 220,\ 380,\ 795)\,\text{fb}\,, \tag{14}$$

$$\sigma(\rho_T, a_T \to Z\pi_T \to \ell^+\ell^- jj) = (205,\ 200,\ 190,\ 145)\,\text{fb}\,, \tag{15}$$

for $\ell = e, \mu$.

The $\rho_T, a_T \to \ell^+\ell^-\ell^\pm\nu_\ell$ mode has been discussed in Refs. [19, 20]. It has the advantages of cleanliness and freedom from jet uncertainties (except $\not{E}_T$ resolution). Standard-model WZ production at the LHC peaks at $M_{WZ} = 300\,\text{GeV}$ [45], near M_{ρ_T}, and this is the dominant background to the $3\ell\nu$ signal. The DØ collaboration searched for this channel using the standard LSTC parameters including $\sin\chi = 1/3$, and excluded it at 95% C.L. up to $M_{\rho_T} \simeq 400\,\text{GeV}$ so long as the $\rho_T \to W\pi_T$ channel is closed [46].

[9] We considered $Q < 80\,\text{GeV}$ to include the a_T, but found that the background increased substantially faster than the signal. The $\rho_T, a_T \to WZ \to \ell^+\ell^- jj$ process is included in this simulation, but it also is removed by the Q-cut.

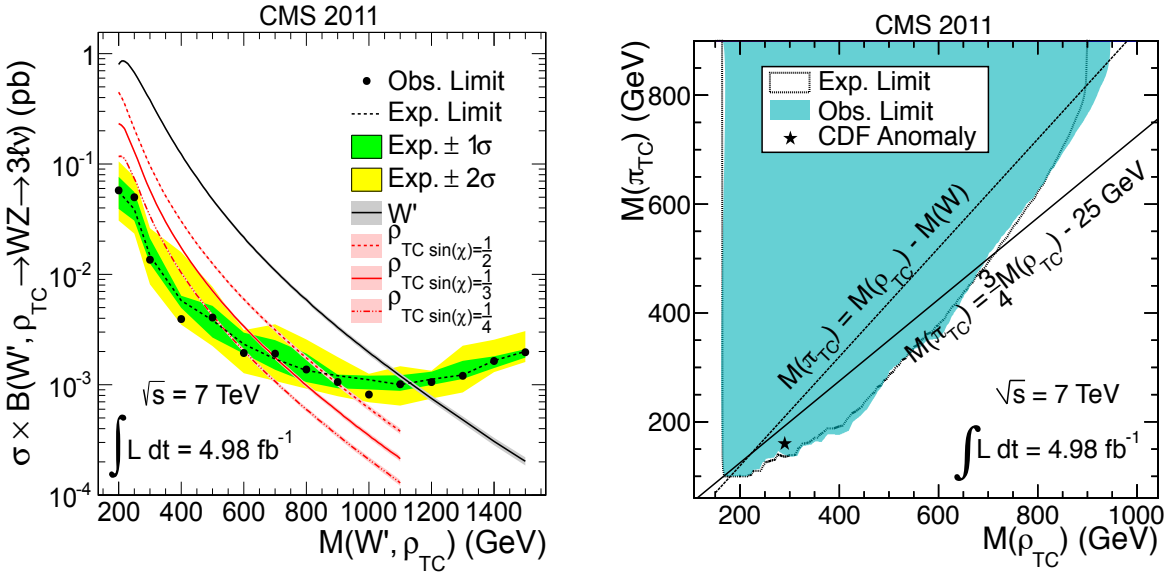

Figure 11: Left: CMS $WZ \to 3\ell\nu$ cross section limits for $\int \mathcal{L}dt = 4.98\,\text{fb}^{-1}$ at $\sqrt{s} = 7\,\text{TeV}$. The LSTC limit curves for $\sin\chi = \frac{1}{4}, \frac{1}{3}, \frac{1}{2}$ assume that $M_{\pi_T} = 0.75 M_{\rho_T} - 25\,\text{GeV}$. Right: Two-dimensional exclusion plot for LSTC with $\sin\chi = 1/3$ as described in the text. The CDF mass point is marked by the star. From Ref. [47].

The ATLAS [48] and the CMS [47] Collaborations have reported searches for a sequential standard model W' and for $\rho_T, a_T \to WZ \to 3\ell\nu$. The CMS Collaboration search used their full $4.98\,\text{fb}^{-1}$ of 7 TeV data [47]. The resulting cross section limits and M_{ρ_T} vs. M_{π_T} exclusion plot are shown in Fig. 11. The LSTC limit curves for $\sin\chi = \frac{1}{4}, \frac{1}{3}, \frac{1}{2}$ assume that $M_{\pi_T} = 0.75 M_{\rho_T} - 25\,\text{GeV}$. This stringent assumption significantly enhances $B(\rho_T^{\pm} \to WZ)$ above its value for the CDF mass point. For the 2-D exclusion plot, standard LSTC parameters, including $\sin\chi = 1/3$, were used. The CDF mass point is indicated by the star. We predicted 21 fb for the signal at 7 TeV. Applying a k-factor of 1.36 in this mass range, CMS excludes $M_{\pi_T} > 140\,\text{GeV}$ at the 95% C.L. for $M_{\rho_T} = 275$–$290\,\text{GeV}$. The 95% upper limit on the cross section at $M_{\rho_T} = 290\,\text{GeV}$ is about 20 fb. Using the CMS k-factor, we estimate that the CDF point is allowed for $\sin\chi \lesssim 0.30$.

The dominant background to $\rho_T, a_T \to WZ \to \ell^+\ell^- jj$ is Z + jets. As can be inferred from Fig. 6 for Wjj production with ATLAS/CDF cuts, the signal will sit at the top of the M_{jj} spectrum. This is what makes the dijet signal in $WW/WZ \to \ell\nu jj$ so difficult to see. On the plus side, since the LSTC and standard model diboson processes have very similar production characteristics, the two signals can be seen with the same cuts and will coincide. We simulated this mode and found a promising set of cuts to extract the $W \to jj$ signal. The basic cuts used for the Zjj signal in Sec. 4 were adopted except that we required $p_T(Z) > 100\,\text{GeV}$, $p_T(jj) > 70\,\text{GeV}$ and $110 < Q = M_{Zjj} - M_W - M_Z < 150\,\text{GeV}$. This

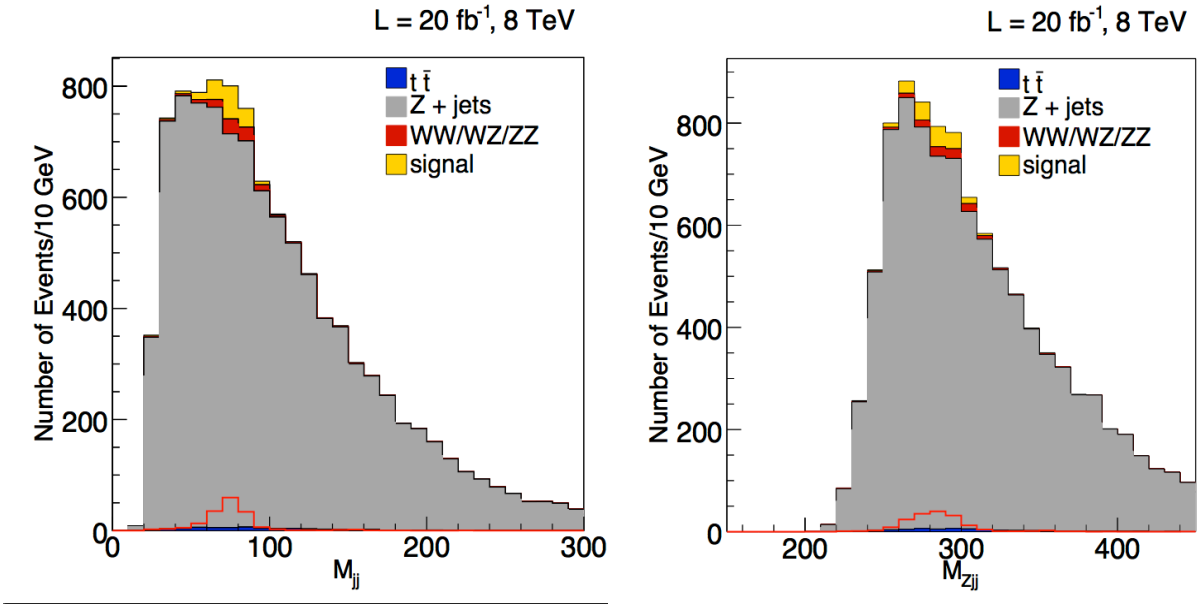

Figure 12: The M_{jj} and M_{Zjj} distributions of $\rho_T^{\pm}, a_T^{\pm} \to WZ \to \ell^+\ell^- jj$ and backgrounds at the LHC for $\sqrt{s} = 8\,\text{TeV}$ and $\int \mathcal{L}dt = 20\,\text{fb}^{-1}$. The cuts used are described in the text. The open red histograms are the π_T and ρ_T signals.

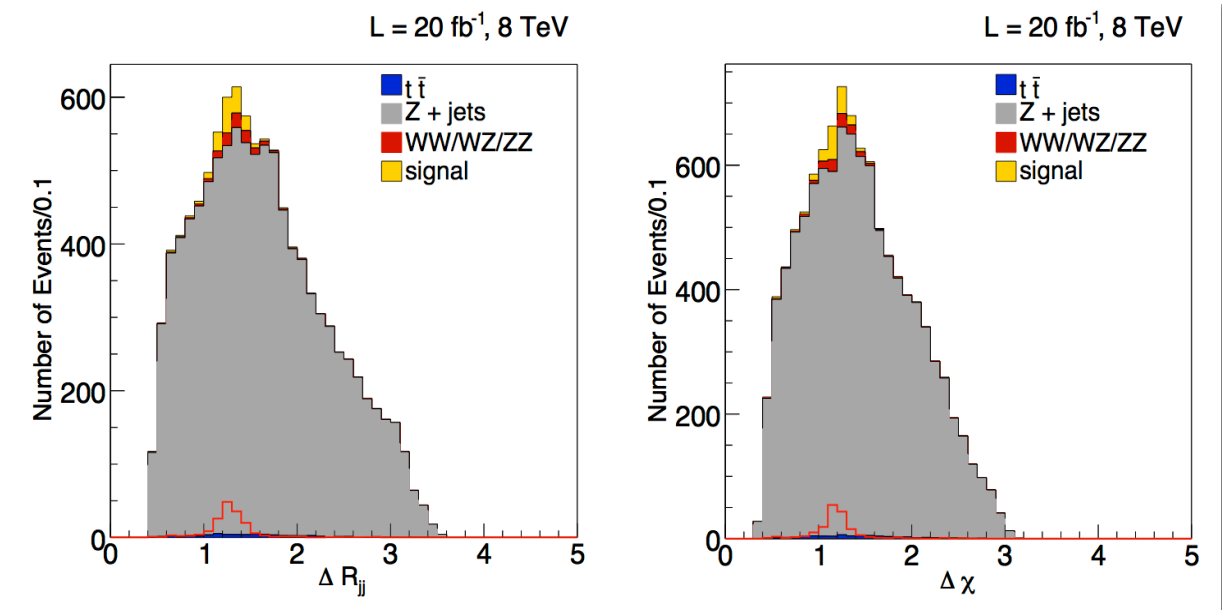

Figure 13: The ΔR and $\Delta\chi$ distributions of $\rho_T^{\pm}, a_T^{\pm} \to WZ \to \ell^+\ell^- jj$ and backgrounds at the LHC for $\sqrt{s} = 8\,\text{TeV}$ and $\int \mathcal{L}dt = 20\,\text{fb}^{-1}$. The cuts used are described in the text. The open red histograms are the signals.

removed some of the a_T contribution for which the nominal $Q = 148\,\text{GeV}$. The mass distributions for $\sin\chi = 1/3$ are shown in Fig. 12 for $\int \mathcal{L}dt = 20\,\text{fb}^{-1}$. The LSTC signal more than doubles the number of standard model $W \to jj$ events in the M_{jj} distribution and it appears that the dijet signal should be observable with such a data set. Including the standard diboson events gives $S/\sqrt{B} = 4.0$ and $S/B = 0.08$ for $60 < M_{jj} < 100\,\text{GeV}$. The M_{Zjj} signal is problematic, but it may be possible to combine its significance with that for $\rho_T \to Z\pi_T \to \ell^+\ell^- jj$. The ΔR and $\Delta\chi$ distributions are in Fig. 13. The narrow LSTC signal and the diboson contribution both peak very near $(\Delta\chi)_{\text{min}} = 2\cos^{-1}(v_W) = 1.21$ and they should be observable if the dijet excess is. The $\ell^+\ell^- jj$ signal is only 60% as large at $\sin\chi = 1/4$ as it is at 1/3. It will be challenging to see it with $20\,\text{fb}^{-1}$ at 8 TeV.

6. Conclusions

Interpreting the dijet excess seen by the CDF Collaboration near 150 GeV in Wjj production as the lightest technipion of the low-scale technicolor process $\rho_T, a_T \to W\pi_T$, we have investigated the observability of this signal by the LHC detectors for $\sqrt{s} = 8\,\text{TeV}$ and $\int \mathcal{L}dt = 20\,\text{fb}^{-1}$. We found that the cuts employed by CDF are not sufficient to confirm the dijet signal with this data set. We constructed cuts more suited for the LHC environment which enhance the $\rho_T, a_T \to \ell\nu jj$ signal to background. However, even though a large "significance", $S/\sqrt{B} = 10.2$, was obtained, $S/B = 0,05$ only. This requires a very good understanding of the $\ell\nu jj$ backgrounds. We believe that this channel is problematic, especially since experimental conditions at the LHC make our theoretical S/B optimistic. Therefore, we doubt the ability of the $\ell\nu jj$ channel to settle the questions of CDF's dijet excess and our interpretation of it [43, 44].

The $\ell^+\ell^- jj$ channel provides a much sharper test of the LSTC hypothesis of the CDF signal, arising as it does from the isospin partner $\rho_T^\pm \to Z\pi_T^\pm$ of the $W\pi_T$ mode. This channel is free of several serious background issues that plague $\ell\nu jj$ production. And its rate is known from the CDF signal's rate without further model-dependent assumptions. For our input masses and model parameters, particularly $\sin\chi = 1/3$, we found $S/\sqrt{B} = 6.2$ and $S/B = 0.11$ for the dijet signal in $120 < M_{jj} < 170\,\text{GeV}$. This channel can be discovered or excluded with the LHC data expected by the end of 2012. The $Z\pi_T^\pm$ channel also benefits from the observability of the sharp edges in the background-subtracted $d\sigma/\Delta R$ and $d\sigma/\Delta\chi$ distributions. These distributions measure the π_T velocity v, providing *independent* confirmations of the $\rho_T \to Z\pi_T$ hypothesis.

Finally, other decay modes of the ρ_T, a_T may be observable at the LHC and provide additional confirmations of LSTC and the parameters we used to describe the CDF signal. The $WZ \to 3\ell\nu$ channel is cleanest of all and its rate is determined from $\sigma(W\pi_T)$ and $\sin\chi$. CMS and ATLAS have sought this signal [48, 47] and, analyzing the full $5\,\text{fb}^{-1}$ set of 7-TeV data, CMS excluded $\sin\chi \gtrsim 0.30$ at the 95% level. This may be close to the limit that the $3\ell\nu$ channel can achieve with this year's data.

Note added: After this paper was completed and in the review process, the ATLAS and CMS collaborations announced the discovery of a new boson X of mass $M_X \cong 125\,\text{GeV}$ and decaying into $\gamma\gamma$ and, with less significance, ZZ and WW in all-lepton modes [49, 50]. The σB's for these modes are roughly consistent with those expected for the standard model Higgs boson H. If the evidence that $X = H$ is strengthened over the next year or so, it will be compelling to make this identification and difficult for the technicolor description of electroweak symmetry breaking, a description that requires no Higgs-like state. On the other hand, if the LHC confirms the CDF signal and our LSTC description of it, it will be just as difficult to understand in the context of the standard model — where no states such as ρ_T and π_T occur. In the meantime, we are exploring the possibility that $X(125)$ is an LSTC bound state with some but not all the properties of the standard model H.

Acknowledgments

We are grateful to K. Black, T. Bose, P. Catastini, V. Cavaliere, C. Fantasia and M. Mangano for valuable conversations and advice. This work was supported by Fermilab operated by Fermi Research Alliance, LLC, U.S. Department of Energy Contract DE-AC02-07CH11359 (EE and AM) and in part by the U.S. Department of Energy under Grant DE-FG02-91ER40676 (KL). KL's research was also supported in part by Laboratoire d'Annecy-le-Vieux de Physique Theorique (LAPTh) and the CERN Theory Group and he thanks LAPTh and CERN for their hospitality.

Appendix: Nonanalytic Threshold Behavior of $d\sigma/d(\Delta R)$

1. Kinematics

We recall first the definition of the angles θ, θ^*, ϕ^* and the relevant coordinate systems. Choose the z-axis as the direction of the incoming quark in the subprocess c.m. frame (or the direction of the harder initial-state parton in the pp collision). In the ρ_T (or a_T) rest frame, θ is the polar angle of the π_T velocity $\boldsymbol{v}$, the angle it makes with the z-axis. Define the xz-plane as the one containing the unit vectors $\hat{\boldsymbol{z}}$ and $\hat{\boldsymbol{v}}$, so that $\hat{\boldsymbol{v}} = \hat{\boldsymbol{x}}\sin\theta + \hat{\boldsymbol{z}}\cos\theta$, and $\hat{\boldsymbol{y}} = \hat{\boldsymbol{z}} \times \hat{\boldsymbol{x}}$. Define a starred coordinate system *in the π_T rest frame* by making a rotation by angle θ about the y-axis of the ρ_T frame. This rotation takes $\hat{\boldsymbol{z}}$ into $\hat{\boldsymbol{z}}^* = \hat{\boldsymbol{v}}$ and $\hat{\boldsymbol{x}}$ into $\hat{\boldsymbol{x}}^* = \hat{\boldsymbol{x}}\cos\theta - \hat{\boldsymbol{z}}\sin\theta$. In this frame, let $\hat{\boldsymbol{p}}_1^*$ be the unit vector in the direction of the jet (parton) making the smaller angle with the direction of $\hat{\boldsymbol{v}}$. This angle is θ^*; the azimuthal angle of $\boldsymbol{p}_1^* = -\boldsymbol{p}_2^*$ is ϕ^*:

$$\cos\theta = \hat{\boldsymbol{z}}\cdot\hat{\boldsymbol{v}}, \quad \cos\theta^* = \hat{\boldsymbol{p}}_1^*\cdot\hat{\boldsymbol{v}}, \quad \tan\phi^* = p_{1y^*}^*/p_{1x^*}^*. \tag{16}$$

The jets from π_T decay are labeled $j = 1, 2$ and they are assumed massless. Let $\zeta_1 = +$ and $\zeta_2 = -$, and $c_\theta = \cos\theta$, $s_\theta = \sin\theta$, etc. The boosted jets in the lab frame are

$$\begin{aligned} p_j^0 &= \tfrac{1}{2}M_{\pi_T}\gamma(1 + \zeta_j v c_{\theta^*}), \\ \boldsymbol{p}_{j\parallel} &= \tfrac{1}{2}M_{\pi_T}\gamma(v + \zeta_j c_{\theta^*})(\hat{\boldsymbol{x}}s_\theta + \hat{\boldsymbol{z}}c_\theta), \\ \boldsymbol{p}_{j\perp} &= \tfrac{1}{2}M_{\pi_T}\zeta_j((\hat{\boldsymbol{x}}c_\theta - \hat{\boldsymbol{z}}s_\theta)s_{\theta^*}c_{\phi^*} + \hat{\boldsymbol{y}}s_{\theta^*}s_{\phi^*}), \end{aligned} \tag{17}$$

where $\gamma = (1 - v^2)^{-\frac{1}{2}}$.

We want to find the minimum of $\Delta R = \sqrt{(\Delta\eta)^2 + (\Delta\phi)^2}$ as a function of c_θ, c_{θ^*} and c_{ϕ^*}. From Eq. (17),

$$\begin{aligned} \Delta\eta = \tfrac{1}{2}\ln\Bigg[&\Big(\frac{1 + vc_{\theta^*} + (v + c_{\theta^*})c_\theta - \gamma^{-1}s_{\theta^*}c_{\phi^*}s_\theta}{1 + vc_{\theta^*} - (v + c_{\theta^*})c_\theta + \gamma^{-1}s_{\theta^*}c_{\phi^*}s_\theta}\Big) \\ &\times\Big(\frac{1 - vc_{\theta^*} - (v - c_{\theta^*})c_\theta - \gamma^{-1}s_{\theta^*}c_{\phi^*}s_\theta}{1 - vc_{\theta^*} + (v - c_{\theta^*})c_\theta + \gamma^{-1}s_{\theta^*}c_{\phi^*}s_\theta}\Big)\Bigg], \end{aligned} \tag{18}$$

and

$$\begin{aligned} \cos(\Delta\phi) &= \frac{\boldsymbol{p}_{T1}\cdot\boldsymbol{p}_{T2}}{p_{T1}\,p_{T2}} \qquad (19) \\ &= \frac{v^2s_\theta^2 - \big(c_{\theta^*}^2\,s_\theta^2 + \gamma^{-2}s_{\theta^*}^2\big(c_\theta^2\,c_{\phi^*}^2 + s_{\phi^*}^2\big)\big) - 2\gamma^{-1}s_{\theta^*}c_{\theta^*}s_\theta\,c_\theta\,c_{\phi^*}}{\Big\{\big[v^2s_\theta^2 + \big(c_{\theta^*}s_\theta + \gamma^{-1}s_{\theta^*}c_{\phi^*}c_\theta\big)^2 + \big(\gamma^{-1}s_{\theta^*}s_{\phi^*}\big)^2\big]^2 - 4v^2s_\theta^2\big(c_{\theta^*}s_\theta + \gamma^{-1}s_{\theta^*}c_{\phi^*}c_\theta\big)^2\Big\}^{1/2}}. \end{aligned}$$

2. Minimum of ΔR

It clearly is hopeless to deal with the analytic expression of ΔR as a function of c_θ, c_{θ^*}, c_{ϕ^*}. However, there is a simple way to bypass it. The quantity

$$\Delta \equiv \frac{M_{\pi_T}^2}{2p_{T1}\,p_{T2}} = \cosh(\Delta\eta) - \cos(\Delta\phi)\,, \tag{20}$$

with $\Delta\eta \geq 0$ and $0 \leq \Delta\phi \leq \pi$, is a monotonically increasing function of ΔR. This is seen by parametrizing

$$\Delta\eta = \Delta R\cos\lambda\,, \quad \Delta\phi = \Delta R\sin\lambda \tag{21}$$

with $\lambda \geq 0$ and $\lambda \leq \pi/2$ if $\Delta R \leq \pi$ or $\lambda \leq \sin^{-1}(\pi/\Delta R)$ if $\Delta R > \pi$. Then

$$\frac{\partial\Delta}{\partial(\Delta R)} = \cos\lambda\sinh(\Delta\eta) + \sin\lambda\sin(\Delta\phi)\,. \tag{22}$$

This is non-negative. It vanishes only for (1) $\Delta R = 0$, which means $\Delta = 0$, and this cannot happen by its definition, Eq. (20), and for (2) $\Delta\eta = 0$, $\Delta\phi = \pi$ meaning $\Delta R = \pi$; the latter is a saddle point. This is the "Col du Delta", but it is one-sided, as shown in Fig. 14.

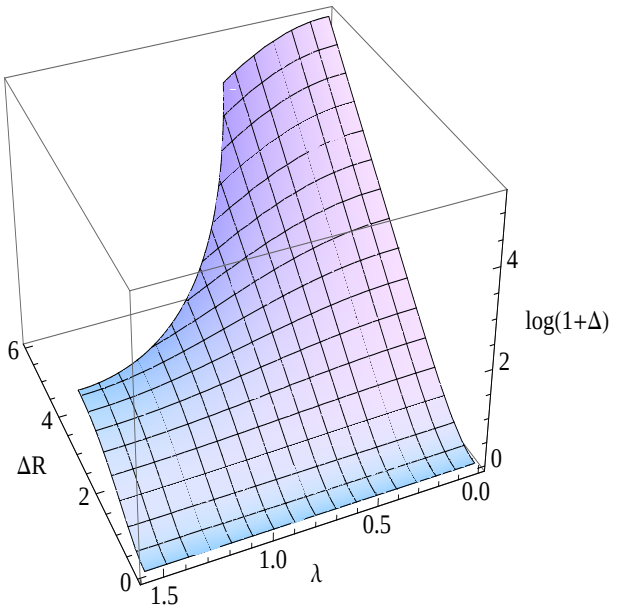

Figure 14: The function $\ln(1+\Delta)$ defined in Eqs. (20,22). The Col du Delta at $\lambda = \pi/2$, $\Delta R = \pi$ is approached along the road $\lambda = \pi/2$. One cannot go over the pass and down the other side for the border is impassable. One must keep climbing along the ridge of increasing ΔR or return via the approach road.

Minimizing ΔR thus amounts to minimizing Δ, which in turn, amounts to maximizing $p_{T1}\,p_{T2}$. This is much simpler to examine than the original problem. We first maximize

$p_{T1}\,p_{T2}$ at fixed c_{θ^*}, then maximize it with respect to c_{θ^*}. Since $p_{Tj} = \sqrt{p_{j0}^2 - p_{jz}^2}$ and p_{j0} depends only on c_{θ^*}, p_{T1} and p_{T2} are separately maximized at fixed c_{θ^*} when $p_{1z} = p_{2z} = 0$. This requires $c_\theta = s_\theta c_{\phi^*} = 0$. Then $p_{T1}\,p_{T2} = (\frac{1}{2}\gamma M_{\pi_T})^2(1 - v^2\cos^2\theta^*)$ is maximized at $c_{\theta^*} = 0$. In conclusion, ΔR is minimized if and only if

$$c_\theta = c_{\theta^*} = c_{\phi^*} = 0\,. \tag{23}$$

This corresponds to two distinct, isolated points in the angular phase space ($\phi^* = \pi/2,\, 3\pi/2$). The degeneracy of the minimum is only discrete. At ΔR's minimum, $\Delta\eta = 0$ and $\Delta\phi = \cos^{-1}(2v^2 - 1) = 2\cos^{-1}(v) \equiv (\Delta\chi)_{\rm min}$, so that

$$(\Delta R)_{\rm min} = (\Delta\chi)_{\rm min} = 2\cos^{-1}(v)\,. \tag{24}$$

3. Local behavior around $\cos\theta = \cos\theta^* = \cos\phi^* = 0$

We now investigate the behavior of ΔR as a function of c_θ, c_{ϕ^*} and c_{θ^*} around its minimum at $c_\theta = c_{\theta^*} = c_{\phi^*} = 0$ by means of a Taylor expansion of at most second order in any of these variables. From, Eqs. (18,19), we obtain

$$\begin{aligned}
(\Delta\eta)^2 &= 4\gamma^{-2}c_{\phi^*}^2 + \mathcal{O}(c^3)\,, \qquad (25)\\
\cos(\Delta\phi) &= \cos(\Delta\chi)_{\rm min} - (1 - \cos(\Delta\chi)_{\rm min})\,v^2(c_\theta^2 + c_{\theta^*}^2) + (1 + \cos(\Delta\chi)_{\rm min})\,\gamma^{-2}c_{\phi^*}^2 + \mathcal{O}(c^3)\,.
\end{aligned}$$

Interpreting the latter equation as:

$$\cos(\Delta\phi) = \cos(\Delta\chi)_{\rm min} - \sin(\Delta\chi)_{\rm min}\,(\Delta\phi - (\Delta\chi)_{\rm min}) + \mathcal{O}((\Delta\phi - (\Delta\chi)_{\rm min})^2) \tag{26}$$

we identify

$$\Delta\phi = (\Delta\chi)_{\rm min} + \left[v^2\tan((\Delta\chi)_{\rm min}/2)\,(c_\theta^2 + c_{\theta^*}^2) - \gamma^{-2}\cot((\Delta\chi)_{\rm min}/2)c_{\phi^*}^2 + \mathcal{O}(c^3)\right]\,. \tag{27}$$

Then

$$\Delta R \equiv \sqrt{(\Delta\eta)^2 + (\Delta\phi)^2} = (\Delta\chi)_{\rm min} + \tfrac{1}{2}\left(b_\theta c_\theta^2 + b_{\theta^*}c_{\theta^*}^2 + b_{\phi^*}c_{\phi^*}^2\right) + \mathcal{O}(c^3)\,, \tag{28}$$

where

$$\begin{aligned}
b_\theta &= b_{\theta^*} = 2v^2\tan((\Delta\chi)_{\rm min}/2) = 2v\gamma^{-1}\,,\\
b_{\phi^*} &= 2\gamma^{-2}\big(2/(\Delta\chi)_{\rm min} - v\gamma\big)\,. \qquad (29)
\end{aligned}$$

The shape of the surface $\Delta R = f(c_\theta, c_{\theta^*}, c_{\phi^*})$ in the neighborhood of the minimum $\Delta R = \Delta\chi_{min}$ is a convex paraboloid with ellipsoidal section whose eigen-directions are parallel to the axes of the coordinates c_θ, c_{θ^*} and c_{ϕ^*}. The curvature is > 0 along each of these axes for all $0 < v < 1$; i.e. there is no flat direction, as expected from the fact the minimum is at isolated point(s).

4. Calculation of the singular part of $d\sigma/d(\Delta R)$

The differential cross section for $\bar{q}q \to \rho_T, a_T \to W/Z\pi_T$, followed by $\pi_T \to \bar{q}q$ is [10]

$$d\sigma = \left[\frac{d\sigma(\bar{q}q \to W/Z\pi_T)}{dc_\theta}\right] B(\pi_T \to \bar{q}q)) \underbrace{\left[\frac{1}{\Gamma(\pi_T \to \bar{q}q)}\frac{d\Gamma(\pi_T \to \bar{q}q)}{dc_{\theta^*}\, dc_{\phi^*}}\right]}_{\left(2\pi\sqrt{1-c^2_{\phi^*}}\right)^{-1}} dc_\theta\, dc_{\theta^*}\, dc_{\phi^*}\,. \quad (30)$$

To compute the distribution in a compound variable ζ, such as $\Delta\chi$ or ΔR, we use a Fadeev-Popov-like trick

$$1 = \int d\zeta\, \delta\left(\zeta - f\left(c_\theta, c_{\theta^*}, c_{\phi^*}\right)\right)\,. \quad (31)$$

where $f(c_\theta, c_{\theta^*}, c_{\phi^*})$ gives the expression of ζ in terms of the phase space variables. The ζ-distribution is then

$$\frac{d\sigma}{d\zeta} \;=\; \int d\sigma(\text{from Eq. (30)})\, \delta\left(\zeta - f\left(c_\theta, c_{\theta^*} c_{\phi^*}\right)\right)\,. \quad (32)$$

Let $\zeta = \Delta R$ be slightly above and close to $(\Delta\chi)_{\min}$, and define $\omega = \Delta R - (\Delta\chi)_{\min}$ to shorten expressions. Solving Eq. (28) with respect to c_{θ^*} gives

$$c_{\theta^*} = \pm\hat{c}_{\theta^*} = \pm\sqrt{\left(\frac{2}{b_{\theta^*}}\right)\left(\omega - \tfrac{1}{2}\left(b_\theta c_\theta^2 + b_{\phi^*} c^2_{\phi^*}\right) + \mathcal{O}(c^3)\right)}\,. \quad (33)$$

Notice that Eq. (33) has to be supplemented by the restriction

$$\omega - \tfrac{1}{2}(b_\theta c_\theta^2 + b_{\phi^*} c^2_{\phi^*} + \mathcal{O}(c^3)) \geq 0\,. \quad (34)$$

Substituting

$$\delta(\Delta R - f(c_\theta, c_{\theta^*}, c_{\phi^*})) = (b_{\theta^*}\hat{c}_{\theta^*})^{-1}\, \left[\delta\left(c_{\theta^*} - \hat{c}_{\theta^*}\right) + \delta\left(c_{\theta^*} + \hat{c}_{\theta^*}\right)\right] \Theta\left[\omega - \frac{1}{2}\left(b_\theta c_\theta^2 + b_{\phi^*} c^2_{\phi^*} + o(c_j^3)\right)\right] \quad (35)$$

in Eq. (31) and integrating over c_{θ^*} leads to the following threshold behavior for the cross section:

$$\left(\frac{d\sigma}{d(\Delta R)}\right)_{\text{threshold}} \;\simeq\; \left[\frac{d\sigma(\bar{q}q \to W/Z\pi_T)}{dc_\theta}\right]_{c_\theta = c_{\theta^*} c_{\phi^*} = 0} B(\pi_T \to \bar{q}q) \quad (36)$$
$$\times \frac{\sqrt{2}}{2\pi}\left(\frac{1}{b_{\theta^*}}\right)^{1/2} \int dc_\theta dc_{\phi^*} \frac{\Theta\left[\omega - \frac{1}{2}\left(b_\theta c_\theta^2 + b_{\phi^*} c^2_{\phi^*} + \mathcal{O}(c^3)\right)\right]}{\left[\omega - \frac{1}{2}\left(b_\theta c_\theta^2 + b_{\phi^*} c^2_{\phi^*} + \mathcal{O}(c^3)\right)\right]^{1/2}}\,.$$

[10] Since there are two points in the $(c_\theta, c_{\theta^*}, c_{\phi^*})$ phase space where ΔR has a minimum, $\theta = \theta^* = \pi/2$ and $\phi^* = \pi/2,\, 3\pi/2$, it is more convenient to use the variable c_{ϕ^*} instead of ϕ^*. This introduces (a) the Jacobian $(1 - c^2_{\phi^*})^{-1/2}$ which is one at $c_{\phi^*} = 0$; and (b) a factor of two to account for the contributions of the two minima in the calculation of the normalization coefficient.

It is convenient to trade c_θ, c_{ϕ^*} for new variables ρ, κ:

$$\rho\cos\kappa = \sqrt{b_\theta/2}\, c_\theta\,, \quad \rho\sin\kappa = \sqrt{b_{\phi^*}/2}\, c_{\phi^*}\,, \qquad (0 \le \rho \le \sqrt{\omega}\,, \quad 0 \le \kappa < 2\pi)\,. \tag{37}$$

The integral in Eq. (36) then yields our final result, the square-root behavior of $d\sigma/d(\Delta R)$ at threshold:

$$\left(\frac{d\sigma}{d(\Delta R)}\right)_{\text{threshold}} \simeq 2^{3/2}\sqrt{\frac{\Delta R - (\Delta\chi)_{\min}}{b_\theta\, b_{\theta^*}\, b_{\phi^*}}}\left[\frac{d\sigma(\bar{q}q \to W/Z\pi_T)}{dc_\theta}\right]_0 B(\pi_T \to \bar{q}q)\,. \tag{38}$$

References

[1] **CDF** Collaboration, T. Aaltonen *et. al.*, "Invariant Mass Distribution of Jet Pairs Produced in Association with a W boson in ppbar Collisions at sqrt(s) = 1.96 TeV," *Phys. Rev. Lett.* **106** (2011) 171801, 1104.0699.

[2] **CDF** Collaboration http://www-cdf.fnal.gov/physics/ewk/2011/wjj/7_3.html.

[3] **D0** Collaboration, V. M. Abazov, "Bounds on an anomalous dijet resonance in W+jets production in ppbar collisions at sqrts =1.96 TeV," *Phys. Rev. Lett.* **107** (2011) 011804, 1106.1921.

[4] A. Annovi, "Physics Beyond the Standard Model, talk at Lepton-Photon 2011, Mumbai, India." 2011.

[5] E. J. Eichten, K. Lane, and A. Martin, "Technicolor at the Tevatron," *Phys. Rev. Lett.* **106** (2011) 251803, 1104.0976.

[6] E. Eichten, K. Lane, and A. Martin, "Testing CDF's Dijet Excess and Technicolor at the LHC," 1107.4075.

[7] E. Eichten, K. Lane, A. Martin, and E. Pilon, "Testing the Technicolor Interpretation of CDF's Dijet Excess at the LHC," 1201.4396.

[8] B. Holdom, "Raising the sideways scale," *Phys. Rev.* **D24** (1981) 1441.

[9] T. W. Appelquist, D. Karabali, and L. C. R. Wijewardhana, "Chiral hierarchies and the flavor changing neutral current problem in technicolor," *Phys. Rev. Lett.* **57** (1986) 957.

[10] K. Yamawaki, M. Bando, and K.-i. Matumoto, "Scale invariant technicolor model and a technidilaton," *Phys. Rev. Lett.* **56** (1986) 1335.

[11] T. Akiba and T. Yanagida, "Hierarchic chiral condensate," *Phys. Lett.* **B169** (1986) 432.

[12] E. Eichten and K. D. Lane, "Dynamical Breaking of Weak Interaction Symmetries," *Phys. Lett.* **B90** (1980) 125–130.

[13] K. D. Lane and E. Eichten, "Two Scale Technicolor," *Phys. Lett.* **B222** (1989) 274.

[14] **D0 Collaboration** Collaboration, V. Abazov *et. al.*, "Search for techniparticles in e+jets events at D0," *Phys.Rev.Lett.* **98** (2007) 221801, hep-ex/0612013.

[15] **CDF Collaboration** Collaboration, T. Aaltonen *et. al.*, "Search for Technicolor Particles Produced in Association with a W Boson at CDF," *Phys.Rev.Lett.* **104** (2010) 111802, 0912.2059.

[16] K. Lane and A. Martin, "An Effective Lagrangian for Low-Scale Technicolor," *Phys. Rev.* **D80** (2009) 115001, 0907.3737.

[17] K. Lane and S. Mrenna, "The collider phenomenology of technihadrons in the technicolor Straw Man Model," *Phys. Rev.* **D67** (2003) 115011, hep-ph/0210299.

[18] E. Eichten and K. Lane, "Low-scale technicolor at the Tevatron and LHC," *Phys.Lett.* **B669** (2008) 235–238, 0706.2339.

[19] G. Brooijmans *et. al.*, "New Physics at the LHC: A Les Houches Report. Physics at Tev Colliders 2007 – New Physics Working Group," 0802.3715.

[20] G. Brooijmans *et. al.*, "New Physics at the LHC. A Les Houches Report: Physics at TeV Colliders 2009 - New Physics Working Group," 1005.1229.

[21] T. Sjostrand, S. Mrenna, and P. Skands, "PYTHIA 6.4 physics and manual," *JHEP* **05** (2006) 026, hep-ph/0603175.

[22] C. Kilic and S. Thomas, "Signatures of Resonant Super-Partner Production with Charged-Current Decays," *Phys. Rev.* **D84** (2011) 055012, 1104.1002.

[23] Q.-H. Cao *et. al.*, "W plus two jets from a quasi-inert Higgs doublet," *JHEP* **08** (2011) 002, 1104.4776.

[24] C.-H. Chen, C.-W. Chiang, T. Nomura, and Y. Fusheng, "A light charged Higgs boson in two-Higgs doublet model for CDF Wjj anomaly," 1105.2870.

[25] J. Fan, D. Krohn, P. Langacker, and I. Yavin, "A Higgsophilic s-channel Z' and the CDF W+2J Anomaly," *Phys. Rev.* **D84** (2011) 105012, 1106.1682.

[26] D. K. Ghosh, M. Maity, and S. Roy, "R parity violating supersymmetric explanation for the CDF Wjj excess," *Phys. Rev.* **D84** (2011) 035022, 1107.0649.

[27] J. F. Gunion, "A two-Higgs-doublet interpretation of a small Tevatron Wjj excess," 1106.3308.

[28] M. R. Buckley, D. Hooper, J. Kopp, and E. Neil, "Light Z' Bosons at the Tevatron," *Phys. Rev.* **D83** (2011) 115013, 1103.6035.

[29] J. Hewett and T. Rizzo, "Dissecting the Wjj Anomaly: Diagnostic Tests of a Leptophobic Z'," 1106.0294v1.

[30] R. Harnik, G. D. Kribs, and A. Martin, "Quirks at the Tevatron and Beyond," *Phys. Rev.* **D84** (2011) 035029, 1106.2569.

[31] B. A. Dobrescu and G. Z. Krnjaic, "Weak-triplet, color-octet scalars and the CDF dijet excess," 1104.2893v1.

[32] A. E. Nelson, T. Okui, and T. S. Roy, "A unified, flavor symmetric explanation for the t-tbar asymmetry and Wjj excess at CDF," *Phys. Rev.* **D84** (2011) 094007, 1104.2030.

[33] F. Yu, "A Z' Model for the CDF Dijet Anomaly," *Phys. Rev.* **D83** (2011) 094028, 1104.0243.

[34] K. Cheung and J. Song, "Baryonic Z' Explanation for the CDF Wjj Excess," *Phys. Rev. Lett.* **106** (2011) 211803, 1104.1375.

[35] E. Eichten, K. D. Lane, and J. Womersley, "Finding low scale technicolor at hadron colliders," *Phys.Lett.* **B405** (1997) 305–311, hep-ph/9704455.

[36] **ATLAS** Collaboration, "Invariant mass distribution of jet pairs produced in association with a leptonically decaying W boson using $1.02\,\text{fb}^{-1}$ of ATLAS data." ATLAS-CONF-2011-097.

[37] M. L. Mangano, M. Moretti, F. Piccinini, R. Pittau, and A. D. Polosa, "ALPGEN, a generator for hard multiparton processes in hadronic collisions," *JHEP* **07** (2003) 001, hep-ph/0206293.

[38] M. Mangano http://mlm.web.cern.ch/mlm/talks/lund-alpgen.pdf, 2004.

[39] J. M. Campbell, R. K. Ellis, and C. Williams, "Vector boson pair production at the LHC," *JHEP* **07** (2011) 018, 1105.0020.

[40] M. Cacciari and G. P. Salam, "Dispelling the N^3 myth for the k_t jet-finder," *Phys. Lett.* **B641** (2006) 57–61, hep-ph/0512210.

[41] J. M. Campbell, A. Martin, and C. Williams, "NLO predictions for a lepton, missing transverse momentum and dijets at the Tevatron," *Phys.Rev.* **D84** (2011) 036005, 1105.4594.

[42] R. Frederix, S. Frixione, V. Hirschi, F. Maltoni, R. Pittau, *et. al.*, "aMC@NLO predictions for Wjj production at the Tevatron," *JHEP* **1202** (2012) 048, 1110.5502.

[43] **CMS** Collaboration, "Study of the dijet invariant mass distribution in $W \to \ell\nu$ plus jets events produced in pp collisions at $\sqrt{s} = 7\,\text{TeV}$." CMS PAS EWK-11-017 [https://cdsweb.cern.ch/record/1431015/files/EWK-11-017-pas.pdf].

[44] C. Collaboration, "Study of the dijet mass spectrum in pp to W + jets events at sqrt(s)=7 TeV," 1208.3477.

[45] E. Eichten, I. Hinchliffe, K. D. Lane, and C. Quigg, "Super Collider Physics," *Rev.Mod.Phys.* **56** (1984) 579–707.

[46] **D0** Collaboration, V. M. Abazov *et. al.*, "Search for a resonance decaying into WZ boson pairs in $p\bar{p}$ collisions," *Phys. Rev. Lett.* **104** (2010) 061801, 0912.0715.

[47] **CMS Collaboration** Collaboration, S. Chatrchyan *et. al.*, "Search for exotic particles decaying to WZ in pp collisions at sqrt(s)=7 TeV," 1206.0433.

[48] **ATLAS Collaboration** Collaboration, G. Aad *et. al.*, "Search for resonant WZ production in the WZ to l nu l' l' channel in sqrt(s) = 7 TeV pp collisions with the ATLAS detector," *Phys. Rev.* **D85** (2012) 112012, 1204.1648.

[49] **The ATLAS Collaboration** Collaboration, G. Aad *et. al.*, "Observation of a new particle in the search for the Standard Model Higgs boson with the ATLAS detector at the LHC," 1207.7214.

[50] **The CMS Collaboration** Collaboration, S. Chatrchyan *et. al.*, "Observation of a new boson at a mass of 125 GeV with the CMS experiment at the LHC," 1207.7235.